Published in final edited form as:

iRadiology. 2024 April ; 2(2): 128–155. doi:10.1002/ird3.62.

Elevating theranostics: The emergence and promise of radiopharmaceutical cell-targeting heterodimers in human cancers

Claudia Chambers[1,2,3], **Broc Chitwood**[1], **Charles J. Smith**[1,2,4,5], **Yubin Miao**[6]

[1]Molecular Imaging and Theranostics Center, Columbia, Missouri, USA

[2]Research Division, Harry S. Truman Memorial Veterans' Hospital, Columbia, Missouri, USA

[3]Department of Chemistry, University of Missouri, Columbia, Missouri, USA

[4]Department of Radiology, University of Missouri School of Medicine, Columbia, Missouri, USA

[5]University of Missouri Research Reactor Center, University of Missouri, Columbia, Missouri, USA

[6]Department of Radiology, University of Colorado Denver, Aurora, Colorado, USA

Abstract

Optimal therapeutic and diagnostic efficacy is essential for healthcare's global mission of advancing oncologic drug development. Accurate diagnosis and detection are crucial prerequisites for effective risk stratification and personalized patient care in clinical oncology. A paradigm shift is emerging with the promise of multi-receptor-targeting compounds. While existing detection and staging methods have demonstrated some success, the traditional approach of monotherapy is being reevaluated to enhance therapeutic effectiveness. Heterodimeric site-specific agents are a versatile solution by targeting two distinct biomarkers with a single theranostic agent. This review describes the innovation of dual-targeting compounds, examining their design strategies, therapeutic implications, and the promising path they present for addressing complex diseases.

Keywords

heterodimer; heterobivalent; hybrid peptide; PSMA; GRPR; $\alpha_v\beta_3$; SST; MSH

Correspondence: Yubin Miao, Charles J. Smith. yubin.miao@cuanschutz.edu, smithcj@health.missouri.edu.

AUTHOR CONTRIBUTIONS

Claudia Chambers: Conceptualization (Supporting); Data Curation (Lead); Visualization (Lead); Writing − Original Draft (Lead); Writing − Review & Editing (Lead). **Broc Chitwood**: Data Curation (Supporting). **Charles J. Smith**: Visualization (Equal); Conceptualization (Equal); Project Administration (Equal); Writing − Original Draft (Supporting); Writing − Review & Editing (Supporting). **Yubin Miao**: Visualization (Equal); Conceptualization (Equal); Project Administration (Equal); Writing − Original Draft (Supporting); Writing − Review & Editing (Supporting).

CONFLICT OF INTEREST STATEMENT

The authors declare no conflict of interest. If authors are from the editorial board of *iRADIOLOGY*, they will be excluded from the peer-review process and all editorial decisions related to the publication of this article.

1 | INTRODUCTION

A groundbreaking approach is emerging in personalized medicine, which employs multimeric peptide-based radiopharmaceuticals for diagnosis and possible therapy of human disease, including cancer. Traditionally, researchers have designed site-directed radiotracers based on a monovalent approach that targets only one biomarker [1, 2]. These radiopharmaceuticals are composed of a solitary targeting vector (such as bioactive peptides, small molecules, nanoparticles, antibodies, or antibody fragments), a pharmacokinetic modifier, a bifunctional chelating agent (BFCA), and a radiometal appropriate for theranostic use (Figure 1). While these radiotracers have exhibited significant success, redirecting to a heterobivalent approach is thought to improve pharmacological properties of the radiotracer and to increase the potential theranostic payload [3–11].

Peptide-based cell targeting radiopharmaceuticals are designed to minimize harm to healthy tissues, distinguishing them from conventional chemotherapy methods for treatment of disease [12]. This synthetic peptide approach is a straightforward process allowing for customization to specifically target biomarkers primarily found on tumor cells in certain human malignancies while sparing normal tissue cells. Additionally, peptide-based radiotracers possess an improved ability to penetrate tumors and their vasculature [13]. Through structural modifications, they can be rapidly eliminated from the bloodstream and non-target tissues to improve pharmacological efficacy. Therefore, ensuring the molecular peptide arrangement is properly configured to have ideal metabolic and biological half-life is essential [14, 15]. To improve the effectiveness of peptide-based radioligands for molecular imaging or targeted radiotherapy (TRT), appropriate radiometals should be chosen. Nuclear characteristics such as half-life, decay mode, and emission profile (Table 1) are important when choosing a radiometal for diagnostic or therapeutic use. For diagnostic imaging, it is important to select either a positron-emitting radioisotope for positron emission tomography (PET) or a gamma-emitting radionuclide for single-photon emission tomography (SPECT). When choosing a radionuclide for TRT, beta or alpha-emitting isotopes are necessary. In addition, the BFCA must have suitable coordination chemistry for the radionuclide of choice to ensure stability of the metal for preclinical and clinical investigations.

A limitation of monovalent cell-targeting agents is their ability to only target a single biomarker or receptor. While radiotracers targeting singular cell surface receptors have demonstrated significant success, these agents lack the versatility to accommodate the possible complexities of malignancies [16]. The inability of these tracers to adapt for diverse cancer stages and varying target expression could limit personalized patient approaches.

There are many supporting factors in using a bivalent multi-targetable approach. For example, utilizing a single agent capable of targeting multiple biomarkers has the potential to enhance sensitivity in detection through improved binding affinity [7–10]. Tumor microenvironment complexity shows diverse levels and varieties of receptor site expression, presenting a challenge for effective targeting. Biomarkers within these malignancies are dynamic, variably expressed throughout the many stages of tumor development, and even differ between individual patients. By directing a single agent toward multiple known biomarkers, research suggests that a wider range of patients can be encompassed, accounting

for expression profiles at all stages [17]. This approach also offers enhanced targeting specificity and theranostic utility enabling precise staging, tailored treatment design, and potential improvements in patient outcomes and quality of life.

This article navigates the complexities of designing and harnessing the power of novel radiotracers that harmonize the dual receptor-targeting actions of these emerging theranostic radiopharmaceuticals for potential usage in clinical applications. This involves understanding the evolution of these synthetic peptide analogs that are optimized for in vivo stability, affinity, specificity, and pharmacokinetic profile. Additionally, advancements in radiochemistry and chelation chemistry have enabled the fine-tuning of these peptides for radiolabeling with various radionuclides, catering to diverse medical applications within nuclear oncology.

2 | SINGLE RECEPTOR CELL-TARGETING AGENTS (MONOVALENT RADIOTRACERS)

2.1 | Somatostatin receptor-targeting radiotracers

Somatostatin (SST) cell-targeting radiotracers have captivated researchers for over 3 decades. Somatostatin is a neuropeptide hormone that is expressed largely in the central and peripheral nervous system. Somatostatin has two native cyclic forms, SST-14, and SST-28. This hormone is produced on delta cell membranes in high quantities of human tissues and malignancies, the highest of which being in the gastrointestinal tract, pancreas, hypothalamus, and central nervous system. Somatostatin also serves as a neuromodulator and neurotransmitter in the central nervous system, affecting neuroendocrine (NE), motor, and cognitive functions, as well as influencing the synthesis of growth factors. Somatostatin plays a crucial role in inhibiting both endocrine and hormone secretion via the five known *G* protein coupled receptors SSTR1–5.

The most clinically useful subtype, SSTR2, is expressed in elevated levels on human neuroendocrine tumors (NET) and neuroendocrine carcinomas [18–20]. The elevated levels of SST receptors on NE neoplasms, as well as SST's antiangiogenic effects has led to the development of radiotheranostic analogs of SST. Peptide receptor radionuclide therapy derivatives have been targeting SST based on the biologically-active tetrapeptide Phe-Trp-Lys-Thr for receptor recognition [21, 22]. While the native hormones SST-14 and SST-28 exhibit significant affinity for all SST receptor subtypes, shorter analogs exclusively engage with the initial subgroup of receptor subtypes SST2, SST3, and SST5. Optimizing analogs of SST has been critical to improve stability, receptor recognition, and biological activity to the different receptor subtypes. Integrating D-amino acids for increased stability onto SST's minimal amino acid sequence has resulted in an octapeptide. This octapeptide is characterized by the active core sequence Phe-D-Trp-Lys-Thr, which forms a six-membered ring via a single disulfide bridge (Figure 2). This peptide is recognized as Octreotide® [23].

In the realm of PET and SPECT molecular imaging, efforts have been made to develop radiotracers that particularly target SST2 positive NET. These radiotracers utilize different radiolabeling strategies and linkers, often based on the octreotate/octreotide peptide

structure. The evolution of SST monovalent radiotracers is detailed, beginning with Lamberts et al.'s 1989 study using ^{123}I-labeled Try^{3}-octreotide [D-Phe-Cys-Phe-D-Trp-Lys-Thr-Cys-Thr(ol)], also known as TOC [24], to visualize endocrine-related tumors [25]. Notable advancements include employing chelators such as diethylenetriaminepentaacetic acid (DTPA) and DOTA (1,4,7,10-tetraazacyclododecane-1,4,7,10-tetraacetic acid) to label radiometals for therapeutic use like ^{90}Y and ^{177}Lu. This paved the way for Peptide receptor radionuclide therapy utilizing agonists such as DOTA-TOC and DOTA-TATE [26, 27]. United States Food and Drug Administration (FDA) approval for the diagnosis and treatment of NETs of three radiotracers, 177Lu-DOTATATE (LUTATHERA®), ^{68}Ga-DOTATATE (NETSPOT®), and 111In-octreotide (SANDOSTATIN®), have marked a significant milestone in the field of theranostics [28]. As a result, a successful theranostic approach targeting these receptors has emerged and has shown positive results in reducing tumor growth and improving patient survival. The success of SST-targeted peptide-based agents has paved the way for exploring similar approaches for other receptor systems, such as Prostate Specific Membrane Antigen (PSMA), melanocortin-1 receptor, bombesin, and integrin complex $\alpha_v\beta_3$.

Researchers have successfully modified the octreotide structure to convert it from an agonist to an antagonist via structural inversion of chirality. The conversion was explored based upon the notion that antagonists bind to a higher number of receptors than agonists in preclinical evaluations, making them a potentially better candidate for tumor targeting. From the very first preclinical evaluation conducted by Ginj et al. [29] the superiority of radiolabeled SST antagonists over agonists was established.

2.2 | Prostate specific membrane antigen targeting radiotracers

Several targeted radiolabeled peptides and small molecules have been innovated to cater to both imaging and therapy requirements for prostate cancer (PCa). One effective approach is targeting PSMA, also known as folate hydrolase I or glutamate carboxypeptidase II. PSMA is a 750-amino acid integral membrane protein predominantly found in the neovasculature of most solid tumors including renal, gastric, pancreatic, breast, brain, and colorectal carcinomas. However, it remains negligible or absent in the normal vascular endothelium of collateral tissues [4, 30]. The ability of PSMA to be rapidly internalized via clathrin-coated pits, coupled with a high incidence of expression on various neoplasias makes this a favorable target in oncologic drug research. PSMA targeting motifs have played a crucial role as both a diagnostic and therapeutic target for PCa research and more recently clinical applications.

PSMA's primary expression in PCa research is observed in the epithelium of prostate tumor cells and, to a lesser extent, in the vasculature of PCa itself. Remarkably, the density per cancer cell reaches approximately 10^6, a figure approximately 1000-fold greater than normal PSMA-expressing tissues located in the kidney, brain, and small intestine [31]. While primarily confined to PCa cell epithelium, the behavior of PSMA changes as the disease progresses to androgen-independent, metastatic stages [32]. This alteration includes upregulation and translocation of PSMA from internal organelles to the cell surface. Notably, upregulated receptor expression has been observed in metastatic lesions located

in lymphatic tissue, bones, and lungs [33]. PSMA's high overexpression on PCa cells, especially advanced-stage carcinomas, as well as swift internalization, make it a suitable target for nuclear imaging and TRT.

Motifs target PSMA through a zinc-cofactor binding site via small molecule enzyme inhibitors. Among these are glutamate-conjugated ureas, thiols, and phosphorus compounds. One of the first FDA-approved imaging agents in 1996 is the Indium-radiolabeled antibody ^{111}In-DTPA-7E11-C5.3, better known as ProstaScint® [34]. While this radiotracer has been widely used for targeting PSMA, limitations of using an antibody-based agent have been challenging. These shortcomings, such as inadequate penetration of solid tumors and slow clearance rates from blood serum and collateral tissues, are being mitigated with the use of radiolabeled peptides and small molecules as alternatives [35]. Glu–urea–glu-based molecules have been designed as an efficient solution in detecting both primary and advanced PCa metastasis. Urea-based ligands showed the most promising results in preclinical trials, while phosphorous and thiol-based ligands showed limited opportunities for clinical use due to poor pharmacokinetic profiles. For example, DUPA (2-[3-(1,3-dicarboxypropyl)-ureido]pentanedioic acid) has been previously labeled with ^{18}F, ^{64}Cu, ^{68}Ga, and ^{86}Y for PET molecular imaging [36]. Of these derivatives, ^{68}Ga-PSMA-11 (Locametz®), was pioneered by Afshar-Oromieh and colleagues in 2012. After Locametz's FDA approval in December of 2020 as well as its endorsement of clinical use by both University of California Los Angeles and University of California San Francisco, interest to clinically use the DUPA derivative for TRT peaked [37, 38]. In 2022, ^{177}Lu-PSMA-617 (Pluvicto®) (Figure 3) was FDA approved for treatment of late stage PCa, showing a reduction ≥50% of PSA levels in PCa patients after their first treatment [39, 40]. Other PSMA targeting small molecules that have demonstrated success in staging PCa in patients have been extensively reported [41–43].

2.3 | Gastrin releasing peptide receptor targeting radiotracers

The neuropeptide bombesin peptide (BBN) is a 14-amino acid peptide with a C-terminal carboxyamide. The Gastrin Releasing Peptide Receptor (GRPR) is a *G* protein-coupled receptor that is well known in the BBN family [44]. This 27-amino acid peptide can be found naturally in the nervous system and the gastrointestinal tract stimulating hormone release and is also overexpressed in various neoplasias including prostate, breast, pancreas, and lung, making it an attractive theranostic target for oncology [45]. Currently, many GRPR radioligands are in preclinical and clinical investigations for the diagnosis and therapy of PCa. The expression of GRPR correlates with tumor grade stage, and other factors [46]. Prostatic tumor cells exhibit elevated levels of GRPR expression, whereas normal prostate tissue demonstrates minimal presence of this receptor [46–50]. GRPR monovalent targeting ligands gained prominence in earlier studies due to their swift internalization within GRP-positive malignancies and their potential for clinical applications. Both BBN antagonist and agonist analogs labeled with various radionuclides have been developed for the purpose of imaging tumors that express GRPR and for TRT [51, 52].

First-generation bombesin analogs have demonstrated prolonged retention within targeted cells due to their internalization properties, suggesting potential enhanced in vivo uptake.

Various radiotracers have been developed and evaluated including [^{68}Ga/^{177}Lu/^{111}In]-AMBA [53–55], ^{18}F-labeled variations including NOTA-8-Aoc-BBN(7–14)NH_2 [56] and Carlucci's [^{18}F]FAl-labeled lanthionine-stabilized BBN analogs [57]. Lane et al. synthesized a series of [^{64}Cu]NO2A-(X)-BBN(7–14)NH_2 agonists where X = AMBA was reported to have superior accumulation, retention, and clearance results in vivo in tumor bearing mice [58]. While the agonists overall demonstrated satisfactory performance, their adverse effects on the gastrointestinal system limited further development.

A shift of strategy began for BBN analogs when a GRP non-internalizing antagonist showed favorable drug disposition characteristics [59]. The second generation development of GRPR radiotracers began when SST2 antagonists demonstrated an increased cell targeting and retention compared to SST2 agonists. Mansi and colleagues synthesized an RM1 (DOTA-Gly-aminobenzoic acid-D-Phe-Gln-Trp-Ala-Val-Gly-His-Sta-Leu-NH_2) antagonist and the In-111 labeled radiotracer to the agonist ^{111}In-AMBA [54]. ^{111}In-RM1 demonstrated superior results propelling a successful study with ^{68}Ga-RM1. Currently, a radiopharmaceutical for RM2 (DOTA-4-amino-1-carboxymethyl-piperidine-D-Phe-Gln-Trp-Ala-Val-Gly-His-Sta-Leu-NH_2) (Figure 4) derivative is undergoing evaluation for approval by the FDA for the treatment of patients with metastatic, castration-resistant, PCa [60, 61]. Studies in four patients who have received ^{68}Ga-RM2 for PET/CT and ^{177}Lu-RM2 for therapy demonstrate high tumor uptake, optimal metabolic clearance/uptake in benign tissues, and no observable side effects. Gastrin Releasing Peptide Receptor + cells also did not show changes in relative expression after being exposed to up to 10 Gy of external beam radiation [62].

Gastrin Releasing Peptide Receptor antagonists offer improved pharmacokinetics compared to agonist radioligands. Although they do not trigger receptor activation upon binding, these antagonists effectively target and remain in GRPR-expressing cancer lesions while quickly clearing from normal organs in both animals and humans [63]. Numerous GRPR ligands have demonstrated successful results in targeting PCa.

2.4 | $\alpha_v\beta_3$ targeting radiotracers

Integrins are glycoproteins consisting of α and β subunits maintaining critical roles in various cellular processes including angiogenesis, cell attachment, and interactions with the extracellular matrix. Angiogenesis allows new blood vessels to form from existing ones acting as a gateway for the tumor cells to transition from dormant to malignant and metastatic. Additionally, it aids in the breakdown of extracellular and interstitial matrices by activation of the matrix metalloproteinase and plasmin. A well-established integrin, $\alpha_v\beta_3$, plays a suspected significant role in the development of multiple cancer metastasis [64]. It is displayed in multiple tumor environments such as malignant melanoma, osteosarcoma, glioblastoma, breast cancer, and PCa. Researchers have coined the minimal amino acid sequence Arg-Gly-Asp (RGD) as the targeting peptide motif for $\alpha_v\beta_3$ receptors overexpressed on tumor and neovasculature [65, 66]. $\alpha_v\beta_3$ is comparatively absent in normal tissues despite mild expression on active endothelial cells and newly formed vessels. $\alpha_v\beta_3$'s comparatively high expression in tumors allows for RGD analogs to target only tissues of interest [67, 68].

The RGD triad has been extensively researched for numerous peptides binding to $\alpha_v\beta_3$ receptors. RGD provides a more than adequate site for conjugation with multiple radionuclides including that is, ^{99m}Tc, ^{111}In, ^{68}Ga, ^{18}F, and ^{64}Cu [69]. Monomeric radiotracers have demonstrated the ability to specifically target $\alpha_v\beta_3$ integrin efficiently, allowing for the potential of diagnostic and therapeutic approaches for cancer [70]. Both linear and cyclic varieties have been researched in attempts to improve binding affinity and pharmacokinetic properties [71, 72].

Several RGD compounds have demonstrated potential for theranostic applications including the cyclodecapeptide scaffold regioselectivity addressable functionalized template (RAFT) [73, 74]. This scaffold displays four c[RGDfK] ligands with a DOTA complex to facilitate radiolabeling with various radionuclides. Among these radionuclides, ^{90}Y and ^{177}Lu for TRT of $\alpha_V\beta_3$-positive tumors were utilized with DOTA, demonstrating high specific tumor accumulation with 10:1 tumor/muscle ratio at 1 h post injection (p.i.) [75]. A cyclam chelator was then replaced on the RAFT scaffold to enable ^{64}Cu PET imaging of $\alpha_V\beta_3$ malignancies [76]. Theranostic RAFT(c[-RGDfK-] 4)–radionuclide conjugates (Figure 5) proved efficient to combine both in vivo cancer diagnostic and therapy in mice in several types of cancers with high tumor penetration and no toxicity [77]. To date, RGD peptides combined with radionuclides have been intensively studied as radiotracers for tumor imaging, with ongoing clinical trials for the PET/CT imaging in various cancers.

2.5 | Melanocortin-1 receptor targeting radiotracers

α-Melanocyte-Stimulating Hormone (α-MSH) is a peptidic pituitary hormone in the family of melanocortin. The 13 amino acid neuropeptide is secreted by melanocytes in response to ultraviolet light and has been extensively studied regarding its interaction with G-protein coupled receptors as well as inducing melanin production. While the primary role of α-MSH is melanin synthesis post-ultraviolet light exposure, it also plays a key role in processes such as repairing DNA damage, production of free radicals, and promoting cell proliferation. Melanocortin-1 receptor (MC1R) is the primary target for α-MSH binding and is found to be significantly overexpressed on primary and metastatic melanoma in comparison to the levels observed in normal cells [78–83]. Thus, α-MSH and its analogs are suitable for MC1R-targeted radiopharmaceutical design and development [84–90].

Naturally occurring α-MSH peptide has a short biological half-life in vivo. Synthetic analogs of α-MSH have been created to overcome this limitation as well as to enhance targeting capabilities. Various modified forms of α-MSH have been developed to enhance biological stability and targeting, including DOTA-[Nle^4, D-Phe^7]α-MSH (DOTA-NDP-MSH), DOTA-NAPamide (Ac-Nle-Asp-His-D-Phe-Arg-Trp-Gly-Lys(DOTA)-NH_2), DOTA-ReCCMSH, DOTA-GlyGlu-CycMSH, and DOTA-Nle-CycMSH$_{hex}$ (Figure 6). Many of these peptides have been successfully labeled with various radiometals such as^{64}Cu, ^{68}Ga, ^{18}F, ^{111}In, ^{99m}Tc, etc [91]. Miao and colleagues developed another class of MC1R-targeted peptide radiopharmaceutical, GGNle-CycMSH$_{hex}$, for melanoma imaging and therapy. Yang et al. conducted initial tests with ^{68}Ga-DOTA-GGNle-CycMSH$_{hex}$ which demonstrated successful detection of human metastatic melanoma lesions, indicating the clinical relevance of MC1R for imaging and potential therapy [80]. Looking into MC1R TRT peptides, Qiao

et al. explored the potential of ^{67}Cu-NOTA-PEG$_2$Nle-CycMSH$_{hex}$ in B16/F10 melanoma bearing C57 mice which displayed favorable biodistribution properties including high tumor uptake (24.10±1.83%ID/g) at 2 h p.i[92]. These ligands, among others, hold promise as platforms for molecular imaging of melanoma, offering enhanced targeting capabilities and potential applications in melanoma-related research and clinical practice. Overall, the efforts to modify and optimize α-MSH and its analogs have significantly expanded their utility in melanoma-targeted imaging and therapeutic strategies.

3 | DUAL RECEPTOR CELL-TARGETING AGENTS (BIVALENT RADIOTRACERS)

3.1 | $\alpha_v\beta_3$-gastrin-releasing peptide receptors cell-targeting radiotracers

Today, research groups have begun to pivot away from the usage of monovalent radioligands, as emerging research into simultaneous, multi-receptor, cell-targeting using heterodimeric conjugates shows potential in enhancing diagnostic capabilities and therapeutic efficacy. Two biomarkers of interest for heterodimeric use are both expressed in very high numbers on the surfaces of PCa cells, $\alpha_v\beta_3$ and GRPR. Targeting both biomarkers with a single radiotracer has been shown to improve retention and accumulation in tumors for TRT and molecular imaging. Along with enhanced pharmacological properties, a multivalent peptide for PCa may also be able to reach a larger cohort of patients [3–6, 11]. This is potentially due to receptor density shift ranging in an order of magnitude when compared to either the GRPR or $\alpha_v\beta_3$ monovalent species alone. Heterodimers that target both $\alpha_v\beta_3$ and GRPR have been shown to be superior to monovalent GRPR or $\alpha_v\beta_3$ [93–97]. For example, using a peptide that allows binding of multiple receptors has shown increased ability to be imaged in cases where one of the receptors is limited by low expression of the targeted biomarker (Table 2).

One of the first research groups to target both GRPR and $\alpha_v\beta_3$ receptors simultaneously was the Chen lab [99]. BBN and RGD were linked with a glutamate amino acid residue to formulate RGD-BBN (Figure 7), which was successfully labeled with ^{18}F and showed promising results in vitro and in vivo [93]. Subsequent to these promising results, NOTA conjugation of the bivalent molecule was evaluated. Production of the ^{68}Ga radiolabeled NOTA-RGD-BBN was substantially more streamlined in comparison to the 18F first generation bivalent molecule and demonstrated more favorable in vivo results [93]. (Figure 8) Biodistribution results of ^{68}Ga-NOTA-RGD-BBN in PC3 xenografted tumor-bearing mice were higher (5.26 ± 0.32%ID/g) at 1 h in comparison to the 18F-RGD-BBN uptake (4.41%ID/g) [98]. To elaborate upon the dual GRPR-$\alpha_v\beta_3$ targeting structure, PEG$_3$-Glu-RGD-BBN was created by attaching a polyethylene glycol (PEG) spacer and 18F-SFB as a synthon to improve the pharmacokinetic properties and enhance ^{18}F labeling yields [100, 101]. Upon successful radiolabeling with a radiochemical purity of ≥99%, the receptor cell binding affinities of ^{18}F-FB-PEG$_3$-Glu-RGD-BBN were observed to align with their respective monomers, Aca-BBN(7–14) and c(RGDyK) [98]. Administration of a blocking agent resulted in complete block of both the integrin and GRPR, confirming the specificity and selectivity of this compound toward both biomarkers of interest. Positron emission tomography images of mice bearing PC3 tumors displayed significant tumor contrast for

up to 120 min p.i., accompanied by a decrease in kidney uptake during the earlier time points. This trend suggests that the compound is primarily cleared through the renal-urinary excretion pathway. Further investigations utilizing positron-emitting agents involved the use of various cell lines. In vivo studies were conducted using breast cancer cell models, namely T47D (GRPR+/low $\alpha_v\beta_3$) and MDA-MB-435 (GRPR-/$\alpha_v\beta_3$+), with ^{18}-F-FB-PEG$_3$-RGD-BBN, ^{68}Ga-NOTA-RGD-BBN, and ^{64}Cu-NOTA-RGD-BBN [97]. PET imaging of each compound was evaluated and quantified to assess pharmacokinetic properties in the blood, liver, kidney, muscle, and tumors of tumor-bearing nude mice. While ^{18}F-FB-PEG3-RGD-BBN exhibited lower tumor uptake at 1 h p.i. (T47D: 1.81 ± 0.34%ID/g; MDA-MB-435: 1.59 ± 0.65%ID/g) compared to the radiometalated conjugates, this conjugate demonstrated significantly lower background uptake in collateral organs [97]. In the T47D (GRPR+) cell line, both ^{64}Cu-NOTA-RGD-BBN and ^{68}Ga-NOTA-RGD-BBN exhibited tumor uptake at 1 h of 2.33 ± 0.59%ID/g and 2.78 ± 0.87%ID/g, respectively. Conversely, in the MDA-MB-435 (GRPR-) cell line, the tumor uptake at 1 h for ^{64}Cu-NOTA-RGD-BBN and 68Ga-NOTA-RGD-BBN was 1.84 ± 0.44%ID/g and 2.24 ± 0.73%ID/g, respectively. Although 64Cu-NOTA-RGD-BBN displayed prolonged liver uptake, it also exhibited the highest liver and kidney accumulation. All of the positron-emitting radiotracers discussed herein effectively targeted the tumors of interest for diagnostic imaging, thus showing some potential for therapeutic applications. Therapeutic efficacy was evaluated using ^{177}Lu-radiolabeled DO3A-RGD-BBN through biodistribution investigations [94]. In mice bearing PC3 xenografted tumors, accumulation of ^{177}Lu-DO3A-RGD-BBN was measured at 5.88 ± 1.12%, 2.77 ± 0.30%, 2.04 ± 0.19%, and 1.18 ± 0.19% ID/g at 0.5, 2, 24, and 48 h p.i., respectively. Notably, rapid clearance from normal tissues led to elevated tumor-to-blood and tumor-to-muscle ratios, highlighting the potential clinical utility of the RGD-BBN theranostic agent.

In 2012, the radiolabeled compound 64Cu-NO2A-RGD-Glu-6-Ahx-BBN(7–14)NH_2 underwent to comprehensive evaluation to assess its affinity for $\alpha_v\beta_3$ and GRPR dual targeting [95]. This study compared CB-TE2A, NO2A, NO3A, and sarcophagine ligands, and variance caused by the slight change in the targeting vector effects changes in the biodistribution. Optimizing the pharmacokinetic modifiers while minimizing the background to produce ideal images. The study of the utilization of NO2A as a BFCA was suggested to mitigate the previously observed elevated kidney uptake associated with RGD/BBN conjugates, as reported by Liu [102–104]. In vivo investigations substantiated this proposition, demonstrating reduced kidney uptake. The uptake at 1 h in the tumor-bearing displayed a value of 4.65 ± 0.78%ID/g representing a higher kidney uptake than Liu's compound of 3.06 ± 0.25%ID/g. Although the compound had higher initial uptake at the 24 h mark, kidney retention was 1.20 ± 0.36%ID/g [95]. This is slightly lower than 1.87 ± 0.41%ID/g at 20 h time point of the anionic analog, showing efficient clearance from the renal system. In addition to lower renal uptake, the new radioligand maintained binding to both biomarkers and achieving heightened radioligand uptake in PC3 xenografts. The study exhibited higher initial tumor uptake at 1 h 3.95 ± 1.04%ID/g compared to Liu's 2.78 ± 0.56%ID/g and both showed an excellent ability to retain activity within tumor sites for several hours post injection [95]. Liver uptake represented in the heterodimeric 64Cu-NO2A-RGD-Glu-6-Ahx-BBN(7–14)NH_2 displayed lower liver retention in comparison to

the monomeric ^{64}Cu-NO2A-6-Ahx-BBN(7–14)NH_2 Notably, the radiolabeled conjugate exhibited rapid excretion through the urinary system and presented remarkable tumor-to-background ratios, demonstrating potential for effective imaging and targeted therapeutic applications.

Until the development of the heterodimeric compound [RGD-Glu-[NO2A]-6-Ahx-RM2], previous dual targeting conjugates aimed at $\alpha_v\beta_3$ and GRPR primarily utilized an agonist-based BBN motif. Antagonistic analogs tend to exhibit enhanced uptake and retention in tumor tissue compared to agonist-based ligands, a phenomenon confirmed by Durkin et al [5], through preclinical investigations involving [RGD-Glu-[^{64}Cu-NO2A]-6-Ahx-RM2]. To assess the pharmacokinetic properties of the peptide conjugate, [RGD-Glu-[^{64}Cu-NO2A]-6-Ahx-RM2] was administered to CF-1 normal mice and tumor-bearing mice. Biodistribution analysis in normal mice over a 1 h period revealed rapid renal clearance, primarily noticeable at the 1 h mark. Negligible uptake was observed in GRPR + pancreas, as expected, and there was no uptake in GRPR-tissues, apart from some accumulation in the liver. Pancreatic uptake was anticipated and observed at the 1 h time point (4.70 ± 1.04%ID/g), with a substantial reduction (0.71 ± 0.08%ID/g) at 4 h. In PC3 tumor-bearing SCID mice, pharmacokinetics and excretion properties mirrored those observed in the normal mouse model. Tumor uptake was measured at 6.37 ± 1.23%ID/g at 4 h post-injection, and this accumulation was retained in the tumor (4.26 ± 1.23%ID/g) up to the 24 h time point [5]. Small animal PET images of the positron-emitting radiotracer in PC3 xenografted mice demonstrated high selectivity and sustained retention in the tumor, yielding high contrast diagnostic images consistent with biodistribution results. Minimal tracer accumulation was noted in collateral tissues.

Stott-Reynolds et al. synthesized and evaluated heterodimeric DOTA conjugate, [RGD-Glu-(DO3A)-6-Ahx-RM2], with the aim of the study being to investigate its potential as a theranostic agent for primary and metastatic PCa (Figure 9) [96]. Metalated analogs, [RGD-Glu-[^{111}In-DO3A]-6-Ahx-RM2] and [RGD-Glu-[^{177}Lu-DO3A]-6-Ahx-RM2], were purified with high yields (>95%) using RP-HPLC. Studies showed high stability for both radioconjugates, showing only a minor variation from the starting material at the 24 h time point. The group believes that this is due to mild, radiolytic degradation. In vitro competitive binding assays were performed with two cell lines, PC-3, and U87-MG, using the unmetaled [RGD-Glu-(DO3A)-6-Ahx-RM2] conjugate and its metalated analogs. Both the unmetalated and conjugate metalated conjugates produced standard sigmoidal curves, depicting a dose-dependent response. The overall IC_{50} values demonstrated effective displacement of the competing radioligands indicating effective binding to both the GRPR and $\alpha_v\beta_3$ targets. High affinity was shown by displacement of ^{125}I-[Tyr^4]-BBN within PC-3 Cells and moderate affinity was shown by displacement of ^{125}I-Echistatin on $\alpha_v\beta_3$ integrin U87-MG cells. A direct comparison between the metalated and the unmetalated compound via competitive displacement assay IC_{50} values in GRPR-expressing PC3 cells was completed. [RGD-Glu-(DO3A)-6-Ahx-RM2] (9.26 ± 0.01 nM) was compared to the metalated conjugates [RGD-Glu-(^{nat}In-DO3A)-6-Ahx-RM2] (5.39 ± 1.37 nM) and [RGD-Glu-(^{nat}Lu-DO3A)-6-Ahx-RM2] (5.83 ± 3.22 nM). The integrin binding affinity with the U87-MG cells demonstrated the unmetalated conjugate to have an affinity of 321 ± 82 nM in comparison to [RGD-Glu-(^{nat}In-DO3A)-6-Ahx-RM2] (372 ± 22.8 nM) or [RGD-Glu-

(^{nat}Lu-DO3A)-6-Ahx-RM2] (346 ± 53 nM) in the same cell line [96]. Other investigator's exploration using U87-MG cells to evaluate monovalent and bivalent conjugates have shown comparable displacement. Biodistribution investigations of [RGD-Glu-(DO3A)-6-Ahx-RM2] using normal CF-1 mice showed rapid clearance of tracer from the blood with only 0.07 ± 0.03%ID/g of the ^{111}In-labeled compound and 0.06 ± 0.06%ID/g of the 177Lu-labeled compound remaining in whole blood by the 4 h time point. These results were seen to be an improvement over the [RGD-Glu-[^{64}Cu-NO2A]-6-Ahx-RM2] antagonist mentioned previously. Notable pancreatic uptake in tumor bearing mice was elevated in comparison to normal mice. However, it was followed by a sharp washout by 24 h. This held a similar trend in comparison to [RGD-Glu-[^{64}Cu-NO2A]-6-Ahx-RM2] [5] previously reported. Monovalent RM2 radioconjugates are known to display this phenomenon due to GRP receptors elevated expression in murine pancreas. In PC3 xenografted SCID mice, [RGD-Glu-(^{111}In-DO3A)-6-Ahx-RM2] remained stable in vivo and demonstrated high retention within the tumor (1 h: 7.02 ± 0.36, 4 h: 6.67 ± 1.05, 24 h: 5.05 ± 0.10%ID/g), with minimal uptake in normal tissues. [RGD-Glu-(^{111}Lu-DO3A)-6-Ahx-RM2] comparably had elevated tumor retention (1 h: 7.77 ± 0.25, 4 h: 7.05 ± 0.31, 24 h: 3.77 ± 0.28%ID/g) [96]. To ensure specificity of the tumor, mice were injected with a known blocking agent (BBN or RGD) 15 min prior to the radiotracer. In both cases, there was an approximate 80% decrease in pancreatic radio-uptake and a 36%–48% decrease in tumor uptake, demonstrating the strong affinity of these compounds for tissues expressing GRPR. The RGD blocking agent produced varying results, exhibited notable inhibitory effects on $\alpha_v\beta_3$ expression in certain mice, while displaying minimal or negligible blocking impact in others. This was due, presumably, to substantially less blocking agent injected than typically used [93, 94]. Small animal SPECT/CT diagnostic images with PC-3 xenografts provided high quality images that provided excellent contrast with minimal tracer in non-tumor tissues at 20 h p.i. This indicated both radiolabeled compounds have high specificity and affinity at GRPR and $\alpha_v\beta_3$ expressing sites. Future $\alpha_v\beta_3$-GRPR bivalent theranostic agents have the potential to serve as promising diagnostic or therapeutic agents for primary and metastatic PCa. Research described herein warrants further investigation to explore alternative chelator/peptide combinations that may optimize the pharmacokinetic profiles of these theranostic agents to enhance clinical utility.

The Missouri research group demonstrated the potential of $\alpha_V\beta_3$-/GRPR-targeting bivalent radiotracers through their investigation of dual-targeting DOTA conjugates, namely [RGD-Glu-[^{177}Lu-DO3A]-6-Ahx-RM2] and RGD-Glu-[^{111}In-DO3A]-6-Ahx-RM2] [96, 105]. These conjugates exhibited exceptional success by displaying high specificity and affinity for the GRPR and $\alpha_V\beta_3$ receptors (Figure 10). Notably, the study emphasized that antagonists might offer advantages over agonists for molecular imaging. However, there is a need for further research to optimize the pharmacokinetic profiles of these promising theranostic agents. Nonetheless, the successes of these radiotracers hold promise for enhancing the efficacy of current PCa treatments and serves as an exemplary model for researchers exploring diverse forms of cancer therapy.

3.2 | $\alpha_v\beta_3$-MC1R targeting radiotracers

Malignant melanoma continues to be the most lethal form of skin cancer with an ever-increasing disease incidence rate. The cancer statistics estimate that 97,610 new cases were diagnosed, and 7990 deaths occurred in the United States in 2023 [106]. Both the melanocortin-1 receptor (MC1R) and the $\alpha_v\beta_3$ integrin receptor are attractive molecular targets for melanoma due to their over-expressions on melanoma cells [78–83]. Initially, radiolabeled alpha-melanocyte-stimulating hormone (α-MSH) peptides were used to target MC1Rs for melanoma imaging [84–90], whereas radiolabeled RGD peptides have been utilized to targeting the $\alpha_v\beta_3$ integrin receptors for melanoma detection [107–112], respectively. Subsequently, the over-expressions of MC1R and $\alpha_v\beta_3$ integrin receptor on melanoma led to the development of radiolabeled RGD-conjugated α-MSH hybrid peptides as dual-receptor-targeting imaging probes for melanoma imaging.

As shown in Figure 11, Yang et al. designed three hybrid peptides with similar molecular weights to demonstrate the dual-receptor-targeting property of an RGD-conjugated α-MSH hybrid peptide [113, 114]. Specifically, the cyclic RGD motif was coupled to the (Arg^{11})CCMSH through a Lys linker to generate RGD-Lys-(Arg^{11})CCMSH to target both MC1 and $\alpha_v\beta_3$ integrin receptors. Meanwhile, the Gly of the cyclic RGD motif was replaced by Ala to yield RAD-Lys-(Arg^{11})CCMSH to target the MC1R only, whereas the MC1R-targeted sequence of His-DPhe-Arg-Trp of the (Arg^{11})CCMSH moiety was scrambled to the Arg-His-Trp-DPhe sequence to generate the $\alpha_v\beta_3$-targeted only RGD-Lys-(Arg^{11})$CCMSH_{scramble}$. They determined the MC1 and $\alpha_v\beta_3$ integrin receptor densities on M21 human melanoma cells and revealed that 1281 MC1 receptors/cell and 96,555 $\alpha_v\beta_3$ integrin receptor/cell presented on M21 human melanoma cells [114], making the M21 human melanoma xenografts a suitable animal model to examine the dual-receptor-targeting capacity of a ^{99m}Tc-labeled RGD-conjugated α-MSH hybrid peptide.

The receptor binding affinities of RGD-Lys-(Arg^{11})CCMSH, RAD-Lys-(Arg^{11})CCMSH and RGD-Lys-(Arg^{11})$CCMSH_{scramble}$ peptides clearly supported their peptide design. The dual-receptor-targeted RGD-Lys-(Arg^{11})CCMSH exhibited 2.0 and 403 nM binding affinities to the MC1 and $\alpha_v\beta_3$ integrin receptors [114], respectively. Meanwhile, RAD-Lys-(Arg^{11})CCMSH maintained its 0.3 nM MC1 receptor binding affinity, but dramatically lost its $\alpha_v\beta_3$ integrin receptor binding affinity by greater than 248-fold compared to RGD-Lys-(Arg^{11})CCMSH. As they anticipated, RGD-Lys-(Arg^{11})CCMSHscramble maintained its 504 nM $\alpha_v\beta_3$ integrin receptor binding affinity but lost its MC1 receptor binding affinity by more than 100-fold compared to RGD-Lys-(Arg^{11})CCMSH [114]. The bio-distribution results of ^{99m}Tc-labeled RGD-Lys-(Arg^{11})CCMSH, RAD-Lys-(Arg^{11})CCMSH and RGD-Lys-(Arg^{11})$CCMSH_{scramble}$ in M21 human melanoma xenografts also strongly supported their peptide design. ^{99m}Tc-RGD-Lys-(Arg^{11})CCMSH exhibited higher M21 melanoma uptake than ^{99m}Tc-RAD-Lys-(Arg^{11})CCMSH or ^{99m}Tc-RGD-Lys-(Arg^{11})$CCMSH_{scramble}$. The M21 melanoma uptake value of ^{99m}Tc-RGD-Lys-(Arg^{11})CCMSH was 2.5 and 2.2 times the tumor uptake value of ^{99m}Tc-RAD-Lys-(Arg^{11})CCMSH and ^{99m}Tc-RGD-Lys-Arg^{11})$CCMSH_{scramble}$ [114], respectively.

Blocking studies also support the dual-receptor-targeting property of ^{99m}Tc-RGD-Lys-(Arg^{11})CCMSH. Either RGD or (Arg^{11})CCMSH peptide co-injection could block 42%

and 57% of the M21 melanoma uptake of ^{99m}Tc-RGD-Lys-(Arg^{11})CCMSH, whereas the co-injection of RGD + (Arg^{11})CCMSH peptide mixture could block 66% of the tumor uptake of ^{99m}Tc-RGD-Lys-(Arg^{11}) CCMSH [114]. Moreover, the M21 melanoma uptake value of ^{99m}Tc-RGD-Lys-(Arg^{11})CCMSH was higher than the sum of the melanoma uptake values of ^{99m}Tc-RAD-Lys-(Arg^{11})CCMSH and ^{99m}Tc-RGD-Lys-(Arg^{11})CCMSH$_{scramble}$, indicating a synergistic (beyond additive) effect between both receptors in M21 human melanoma for ^{99m}Tc-RGD-Lys-(Arg^{11})CCMSH [114]. The potential synergistic effect between the MC1 and $\alpha_v\beta_3$ integrin receptors might promote the elevation of the regional peptide concentration of ^{99m}Tc-RGD-Lys-(Arg^{11}) CCMSH in the proximity of the MC1 and $\alpha_v\beta_3$ integrin receptors. ^{99m}Tc-RGD-Lys-(Arg^{11})CCMSH bound to either MC1 or $\alpha_v\beta_3$ integrin receptor would be in close proximity of other available MC1 or $\alpha_v\beta_3$ integrin receptors, facilitating further binding of ^{99m}Tc-RGD-Lys-(Arg^{11})CCMSH molecule somewhat dissociated from the current binding receptor to other available MC1 or $\alpha_v\beta_3$ integrin receptors in close proximity.

Despite the dual-receptor-targeting property of ^{99m}Tc-RGD-Lys-(Arg^{11})CCMSH in M21 human melanoma-xenografted nude mice, ^{99m}Tc-RGD-Lys-(Arg^{11})CCMSH exhibited remarkably high non-specific renal uptake (67.06 ± 16.53%ID/g at 2 h p.i.) [114]. Co-injection of L-Lysine reduced the renal uptake of ^{99m}Tc-RGD-Lys-(Arg^{11})CCMSH by 52% at 2 h p.i. without affecting tumor uptake, suggesting that the overall positive charge of ^{99m}Tc-RGD-Lys-(Arg^{11})CCMSH substantially contributed to its non-specific renal uptake. As shown in Figure 11, three Arg residues and one Lys linker represent the positive charges of ^{99m}Tc-RGD-Lys-(Arg^{11})CCMSH. The Arg residues are critical to the MC1 or $\alpha_v\beta_3$ integrin receptor binding. To reduce the non-specific renal uptake, Xu et al. replaced the positively charged Lys linker of ^{99m}Tc-RGD-Lys-(Arg^{11})CCMSH with neutral 8-aminooctanoic acid (Aoc) or polyethylene glycol (PEG_2) to yield ^{99m}Tc-RGD-Aoc-(Arg^{11})CCMSH and ^{99m}Tc-RGD-PEG_2-(Arg^{11})CCMSH [115]. Interestingly, the bio-distribution results in M21 melanoma xenografts revealed that the substitution of the Lys linker with Aoc and PEG_2 linker significantly reduced the renal uptake of ^{99m}Tc-RGD-Aoc-(Arg^{11})CCMSH and ^{99m}Tc-RGD-PEG_2-(Arg^{11}) CCMSH by 58% and 63% at 2 h p.i. The renal uptake of ^{99m}Tc-RGD-Aoc-(Arg^{11})CCMSH and ^{99m}Tc-RGD-PEG_2-(Arg^{11})CCMSH was 27.93 ± 3.98 and 22.01 ± 9.89%ID/g at 2 h p.i. Meanwhile, ^{99m}Tc-RGD-Aoc-(Arg^{11})CCMSH displayed similar M21 melanoma uptake as ^{99m}Tc-RGD-Lys-(Arg^{11})CCMSH at 2 h p.i [115].

Xu et al. further examined the effect of the linker [Lys, Arg, Aminohexanoic acid (Ahx), βAla, Gly] on the bio-distribution properties of ^{99m}Tc-RGD-Linker-(Arg^{11}) CCMSH peptides in B16/F1 melanoma-bearing C57 mice [116–118]. Interestingly, as shown in Figure 12, the replacement of Lys with Arg dramatically reduced the renal uptake of ^{99m}Tc-RGD-Arg-(Arg^{11})CCMSH by 36% at 2 h p.i. as compared to ^{99m}Tc-RGD-Lys-(Arg^{11})CCMSH [116]. Moreover, the replacement of Lys with Ahx, βAla and Gly tremendously decreased the renal uptake of ^{99m}Tc-RGD-Ahx-(Arg^{11})CCMSH, ^{99m}Tc-RGD-βAla-(Arg^{11})CCMSH and ^{99m}Tc-RGD-Gly-(Arg^{11})CCMSH by 75%, 76% and 69% at 2 h p.i. as compared to ^{99m}Tc-RGD-Lys-(Arg^{11})CCMSH, respectively [114, 117]. The elimination of Lys also reduced the renal uptake of ^{99m}Tc-RGD-(Arg^{11})CCMSH by 64% at 2 h p.i. as compared to ^{99m} Tc-RGD-Lys-(Arg^{11})CCMSH. The elimination or replacement

of the positively charged Lys linker with neutral hydrocarbon linkers partially shielded the electrostatic interaction between the positively charged peptide molecules and negatively charged tubule cells, leading to a reduction in renal accumulation.

While the switch from RGD to RAD in RGD-Lys-(Arg^{11})CCMSH decreased the $\alpha_v\beta_3$ integrin receptor binding affinity by 248-fold, surprisingly, the switch from RGD to RAD dramatically enhanced the MC1 receptor binding affinity of RAD-Lys-(Arg^{11})CCMSH as compared to RGD-Lys-(Arg^{11})CCMSH (0.3 vs. 2.0 nM) in M21 melanoma cells [114]. It is worthwhile to note that only MC1 receptors (rather than $\alpha_v\beta_3$ integrin receptors) are overexpressed on B16/F1 cells [114]. Therefore, the selection of the B16/F1 melanoma model could minimize the contribution of $\alpha_v\beta_3$ integrin receptors to the melanoma uptake of dual receptor-targeting ^{99m}Tc-RGD-Lys-(Arg^{11})CCMSH. Interestingly, such improvement in the MC1 receptor binding affinity eventually increased the B16/F1 melanoma uptake of ^{99m}Tc-RAD-Lys-(Arg^{11}) CCMSH as compared to ^{99m}Tc-RGD-Lys-(Arg^{11})CCMSH. The B16/F1 tumor uptake of ^{99m}Tc-RAD-Lys-(Arg^{11}) CCMSH was 1.5, 1.3 and 1.4 times the tumor uptake of ^{99m}Tc-RGD-Lys-(Arg^{11})CCMSH at 0.5, 2 and 4 h p.i., respectively [119].

The structural difference between ^{99m}Tc-RAD-Lys-(Arg^{11})CCMSH and ^{99m}Tc-RGD-Lys-(Arg^{11})CCMSH is Ala and Gly. Specifically, Ala has one more methyl group than Gly. Such minor structural differences from Gly to Ala resulted in stronger MC1R binding affinity and higher B16/F1 melanoma uptake for ^{99m}Tc-RAD-Lys-(Arg^{11}) CCMSH [119]. It was desirable to understand how the replacement of Gly with other amino acids could affect the melanoma targeting and pharmacokinetic properties of ^{99m}Tc-RXD-Lys-(Arg^{11})CCMSH peptides. Therefore, the Gly was replaced by a variety of amino acids including Thr, Val, Ser, Nle, Phe and DPhe to yield a class of RXD-Lys-(Arg^{11})CCMSH peptides [120, 121]. The introduction of Thr, Val, Ser, Nle, Phe and DPhe generated different impact on the MC1 receptor binding affinities of the peptides on B16/F1 melanoma cells. The MC1R binding affinities of the peptides ranged from 0.7 to 3 nM. Among these six peptides, RTD-Lys-(Arg^{11})CCMSH displayed the strongest MC1R binding affinity (0.7 nM), whereas RNleD-Lys-(Arg^{11})CCMSH exhibited the weakest MC1R binding affinity (3 nM). Although the -His-DPhe-Arg-Trp-motif is the binding moiety to MC1 receptor, the difference in receptor binding affinity suggested that the amino acid at this position subtly interacted with the receptor binding moiety. Such subtle interactions were likely related to the flexibility of lactam bonds among amino acid residues in the peptides.

^{99m}Tc-RTD-Lys-(Arg^{11})CCMSH, ^{99m}Tc-RVD-Lys-(Arg^{11})CCMSH and ^{99m}Tc-RSD-Lys-(Arg^{11})CCMSH exhibited comparably high receptor-mediated B16/F1 melanoma uptake to ^{99m}Tc-RAD-Lys-(Arg^{11})CCMSH. However, ^{99m}Tc-RVD-Lys-(Arg^{11})CCMSH and ^{99m}Tc-RSD-Lys-(Arg^{11})CCMSH displayed similar lower renal uptake than ^{99m}Tc-RTD-Lys-(Arg^{11})CCMSH by approximately 30% at 0.5, 2, and 4 h p.i [120, 121]. Not surprisingly, ^{99m}Tc-RFD-Lys-(Arg^{11})CCMSH and ^{99m}Tc-RfD-Lys-(Arg^{11})CCMSH showed much higher liver and renal up-take than ^{99m}Tc-RSD-Lys-(Arg^{11})CCMSH. Despite the high B16/F1 melanoma uptake associated with some ^{99m}Tc-RXD-Lys-(Arg^{11})CCMSH peptides, it was desirable to address the issue of high renal uptake of ^{99m}Tc-RXD-Lys-(Arg^{11})CCMSH peptides (67–135%ID/g at 2 h p.i.). Co-injection of L-lysine dramatically decreased the renal up-take of ^{99m}Tc-RTD-Lys-(Arg^{11})CCMSH, ^{99m}Tc-RVD-Lys-(Arg^{11})CCMSH and

^{99m}Tc-RSD-Lys-(Arg^{11})CCMSH by 40%–50%, suggesting that the overall positive charges of the ^{99m}Tc-RXD-Lys-(Arg^{11})CCMSH peptides played key roles in their non-specific renal uptake.

The substitution of the positively charged Lys linker with a neutral βAla yielded three ^{99m}Tc-RXD-βAla-(Arg^{11})CCMSH peptides, whereas the further replacement of positively charged Arg in RAD moiety generated three ^{99m}Tc-XAD-βAla-(Arg^{11})CCMSH peptides [122]. The substitution of the substitution of the positively charged Lys linker with a neutral βAla reduced the overall positive changes of ^{99m}Tc-RXD-βAla-(Arg^{11}) CCMSH peptides. Meanwhile, the modification of positively charged Arg in the RAD moiety further decreased the overall positive charge of ^{99m}Tc-XAD-βAla-(Arg^{11}) CCMSH peptides. The substitution of the Lys linker with a βAla linker resulted in the reduction in tumor uptake for ^{99m}Tc-RXD-βAla-(Arg^{11})CCMSH peptides by 21%–45% in B16/F1 melanoma-bearing C57 mice at 2 h p.i. as compared to ^{99m}Tc-RAD-Lys-(Arg^{11})CCMSH [121, 122]. Specifically, the tumor uptake of ^{99m}Tc-RAD-βAla-(Arg^{11})CCMSH (15.66 ± 6.19%ID/g) was 79% of the tumor uptake of ^{99m}Tc-RAD-Lys-(Arg^{11})CCMSH at 2 h p.i. (11, 12). The substitution of the Lys linker with a β-Ala linker dramatically decreased the renal uptake of ^{99m}Tc-RXD-β-Ala-(Arg^{11})CCMSH peptides by 64%–79% in B16/F1 melanoma-bearing C57 mice at 2 h p.i. as compared to ^{99m}Tc-RAD-Lys-(Arg^{11})CCMSH. The renal uptake of ^{99m}Tc-RAD-βAla-(Arg^{11})CCMSH (20.18 ± 3.86%ID/g) was 22% of the tumor uptake of ^{99m}Tc-RAD-Lys-(Arg^{11}) CCMSH at 2 h p.i. Co-injection of 15 mg of L-lysine further reduced the renal uptake of ^{99m}Tc-RAD-βAla-(Arg^{11})CCMSH from 20.18 ± 3.86%ID/g to 13.06 ± 3.62% ID/g at 2 h p.i. without significantly affecting the tumor uptake. However, the replacement of Arg in ^{99m}Tc-RAD-βAla-(Arg^{11})CCMSH with Nle and Glu did not further decrease the renal uptake [122].

The representative SPECT/CT images of ^{99m}Tc-RGD-Lys-(Arg^{11})CCMSH and ^{99m}Tc-RGD-Aoc-(Arg^{11})CCMSH on M21 human melanoma-xenografted nude mice, ^{99m}Tc-RGD-Arg-(Arg^{11})CCMSH and ^{99m}Tc-RAD-βAla-(Arg^{11})CCMSH on B16/F1 melanoma-bearing C57 mice are summarized in Figure 13. Both M21 and B16/F1 melanomas could be clearly visualized and the effect of linker on the renal uptake were demonstrated in small animal SPECT images (Figure 13).

Both receptor density and receptor binding affinity are crucial factors to consider in the development of an imaging probe targeting two receptors (MC1 and $\alpha_v\beta_3$ integrin receptors) overexpressed on M21 human melanoma cells. Potential synergistic effect between two receptors and the delicate balance in dynamic ligand-receptor binding play roles in the success of a dual receptor-targeting peptide as well. Despite the relatively low MC1 receptor density (1281 receptors/cell) and high nanomolar $\alpha_v\beta_3$ integrin receptor binding affinity (403 nM), high $\alpha_v\beta_3$ integrin receptor density (96,555 receptor/cell) and low nanomolar MC1 receptor binding affinity (2.0 nM) might substantially contribute to the successful visualization of M21 human melanoma using ^{99m}Tc-RGD-Lys-(Arg^{11})CCMSH as an imaging probe. Presumably, higher MC1R density and stronger $\alpha_v\beta_3$ integrin receptor binding affinity would further enhance the success of dual-receptor-targeted radiolabeled peptides for melanoma detection (Table 3).

3.3 | $\alpha_v\beta_3$-SST2 cell-targeting radiotracers

A critical component of tumoral growth and development involves angiogenesis. Researchers have grown interested in the possibility of regulating angiogenesis in hopes of developing an improvement to modern-day cancer therapy. Most of the current research pertains to targeting cancer cells through monovalent conjugates. The De Jong group is one of the very few groups striving to enhance the pharmacokinetic profiles of potential drugs against cancer through bivalent methodologies [123–125]. Using a combination of two distinct sequences of $\alpha_v\beta_3$ targeting RGD and SST2 targeting analogs, the group believes a dual targeting heterodimer could have therapeutic potential. SST2 receptors, significantly upregulated on various cancer cell surfaces, notably those of NE origin, remain unresponsive to conventional therapeutic regimens including chemotherapy and external beam radiation. $\alpha_v\beta_3$ receptors exhibit a similar upregulation. Combining an agent to target both receptors simultaneously and leveraging the synergistic effects of an apoptosis-inducing factor, such as the $\alpha_v\beta_3$-targeting RGD motif, may amplify radiotherapeutic efficacy across a spectrum of cancers.

One of the initial reports of a SST-$\alpha_v\beta_3$ bivalency approach was by Bernard et al. [123], featuring the bivalent peptide, RGD-DTPA-Tyr^3-octreotate (Figure 14). This conjugate comprises three main components: RGD for inducing apoptosis potential, SST targeting agent Tyr^3-octreotate for enhanced internalization, and the bifunctional chelator DTPA for radiolabeling. RGD-DTPA-Tyr^3-octreotate was radiolabeled with 111In and evaluated for specificity in vivo and in vitro. The in vitro internalization in SST2 positive CA20948 tumor cells of the radiolabeled hybrid analogue appeared to be a rapid process, blockable by excess unlabeled octreotide, indicating an SST2-specific mechanism. Biodistribution results of RGD-^{111}In-DTPA-Tyr^3-octreotate in rats xenografted with CA20948 or $\alpha_v\beta_3$-positive AR42J tumors agreed with the uptake and internalization data. The bivalent radiotracer demonstrated a tumor uptake like that of monovalent radiolabeled octreotate in vivo but demonstrated high renal uptake as well, only partially blockable after injecting octreotide. Pharmacokinetic properties of RGD-^{111}In-DTPA-Tyr^3-octreotate were directly compared to RGD-^{111}In-DOTA-Tyr^3-octreotate, revealing higher renal radiometal accumulation in the kidney for the DTPA conjugate in comparison to the DOTA conjugate [123]. While the radiolabeled bivalent peptide showed high tumor uptake and retention, the substantial renal accumulation makes this drug impractical for future theranostic application. To mitigate this, the effect of injecting D-lysine along with the radiotracers to reduce kidney uptake was evaluated. Analyses included the co-injection of 400 mg/kg of D-lysine to determine the possibility of decreasing renal uptake. Results show a reduction of RGD-^{111}In-DTPA-Tyr^3-octreotate by 40% within the renal system [123].

Capello et. al. [124] further investigated this bivalent analogue through in vitro assays to analyze cell death activity. Colony forming assays employing various cell lines were used to evaluate tumoricidal effects based on apoptosis, linked with caspase-3 activity. The bivalent RGD-^{111}In-DTPA-Tyr^3-octreotate conjugate exhibited significantly increased apoptosis compared to either ^{111}In-RGD or ^{111}In-DTPA-Tyr^3, both of which had minimal effect on cell survival [124]. Due to high renal uptake, the bivalent analogue is deemed inappropriate for therapeutic use at this stage of development (Table 4). However, unlabeled

RGD-DTPA-octreotate continues to induce apoptosis for tumor-induced angiogenesis which indicates therapeutic potential for this compound [125].

3.4 | $\alpha_v\beta_3$-PSMA cell-targeting radiotracers

Prostate Specific Membrane Antigen and integrin $\alpha_v\beta_3$, are biomarkers that are overexpressed on the cell surface of certain tumor epithelium as well as most solid tumor neovasculature and are critical targets for cancer therapy. Their overexpression in a variety of malignancies makes them attractive targets for simultaneous targeting, enhancing affinity toward numerous cancer types across different patient cohorts. The Pomper lab has developed a heterobivalent agent, EUKL-cRGDfK-NH_2 functionalized with either a near-infrared dye (IRDye800CW) or bifunctional chelator DOTA for theranostic applications [126]. These agents demonstrate multitargeting capabilities by incorporating a low molecular weight PSMA-targeting urea-based PSMA inhibitor and a cyclic RGD (cRGDfK) $\alpha_v\beta_3$-targeting moiety with a β-glutamic acid linker into a single construct. In vitro assays utilizing near-infrared cell-based binding assays involving PSMA-positive PC3-PIP and $\alpha_v\beta_3$-expressing U87-MG cells were conducted to assess the binding affinities of the conjugated heterobivalent probe. The results showed comparable affinities to their respective monovalent compounds, validating the efficacy of the construct. Subsequent in situ ligand energy minimization algorithm experiments were completed to predict the binding mode of the DOTA-conjugated heterobivalent agent. These computational analyses supported a model describing the conformations adopted by the agent, enabling its binding to both protein targets. Subsequently, in vivo optical assays were conducted using EUKL-cRGDfK-NH2-IRDye800 on PC3-PIP, U87-MG, and PC3 (negative control) xenografted mice. These studies demonstrated high uptake in both PSMA and $\alpha_v\beta_3$ malignancies, and the uptake was effectively blockable using a respective cell line-specific blocking agent, affirming the targeting specificity of the heterobivalent agent. These findings collectively underline the promising potential of EUKL-cRGDfK-NH_2 for targeted imaging and therapy in diverse cancer contexts, highlighting its potential clinical translational value.

3.5 | Prostate specific membrane antigen-gastrin-releasing peptide receptors cell-targeting radiotracers

Since 2014, overall incidence rates of PCa, the second most leading cancer in men, have been increasing by roughly 3% annually [127]. For advanced-stage disease, a 5% increase has been observed each year with only a 32% 5 year survival for patients with metastatic PCa. In 2023, it is estimated that there will be 34,700 male fatalities attributed to metastatic disease, with a mortality rate of 18.8% among affected patients [106]. GRPR and PSMA are promising molecular targets for PCa radiopharmaceuticals due to their heightened expression on PCa cells. Monovalent species of PSMA-targeting radiotracers are successful and available for clinical use, while RM2 GRPR-targeting tracers are awaiting FDA approval. Despite their success, the inherent heterogeneity of tumors presents a challenge for increasing the specificity of monovalent targeted radiotracers. Gastrin Releasing Peptide Receptor expression is elevated in earlier stages of PCa, while PSMA is upregulated in locoregional or late-stage disease [128]. An investigation directly comparing the performance of ^{68}Ga-RM2, a GRPR-targeted radiotracer, and two different drugs, a PSMA-targeted agent, revealed that 43 lesions in only 18 of the 50 patients could

be detected by one of the radiotracers. This culminated in the development of a single heterobivalent conjugated radiotracer targeting both GRPR and PSMA to effectively target multiple bio-markers, thereby enhancing its applicability in the detection, staging, and treatment of both primary and metastatic PCa.

Studies investigating PSMA-BBN-based heterodimers have been documented and have produced diverse outcomes (Table 5). Eder et al. [129] have prepared, via fmoc-solid phase peptide synthesis, a urea-based PSMA inhibitor with the nonapeptide BZH3 for GRPR targeting to yield the compound Glu-urea-Lys(Ahx)-HBED-CC-BZH3 (Figure 15). This bispecific molecule was radiolabeled with ^{68}Ga and showed strong binding affinity to both PSMA and GRPR in competitive displacement as-says (25.0 ± 5.4 nM and 9.0 ± 1.8 nM, respectively) as well as pharmacokinetic uptake and excretion closely resembling their respective monomeric building blocks [129]. In biodistribution investigations, GRPR+ AR42J xenografted mice showed uptake of 5.4 %ID/g and PSMA+ LNCaP bearing mice showed 3.3 %ID/g accumulation in tumors with high PSMA-mediated uptake values in the kidneys and spleen. Subsequently, pharmacokinetic properties of this molecule were optimized by incorporating hydrophilic linkers between the HBED chelator and the BXH3 GRPR-targeting moiety [134]. The three amino acid linkers tested, $(HE)_n$ (n = 0–3) were made up of positively charged His and negatively charged Glu to decrease the relatively high radiotracer uptake in the kidneys and spleen. The results of this modified low-molecular weight heterodimer $HE_{1–3}$ showed decreased liver and spleen accumulation and also a reduction in kidney uptake (>50%) in comparison to the first-generation radiotracer [129, 134].

A multipurpose, bivalent [DUPA-6-Ahx-(NODAGA)-5-Ava-BBN(7–14)NH_2] radioconjugate labeled with ^{64}Cu for PCa imaging was developed by the Smith research lab in 2014 [4]. Specifically, urea-based PSMA targeting DUPA ((2-[3-(1,3-dicarboxypropyl)-ureido]pentanedioic acid))and GRPR targeting BBN(7–14)NH_2 were synthesized via solid-phase peptide synthesis, followed by the manual conjugation of a NODAGA chelator to the ε amine of lysine. Cyclotron produced ^{64}Cu is an attractive radiometal for PET molecular imaging because of its ideal nuclear properties, making it useful in vivo. In vitro assays including fluorescence microscopy and competitive binding were performed to ensure specifi-city and selectivity. Fluorescence microscopy of a Rhodamine-B derivative conducted at 590 nm demonstrated the successful targeting and biomarker specificity for both GRPR and PSMA expressing cells using a single radioligand. Small animal PET molecular images acquired using [DUPA-6-Ahx-(^{64}Cu-NODAGA)-5-Ava-BBN(7–14)NH2] illustrated the efficacy of the radiotracer in detecting PCa. Binding affinity for LNCaP homogenized cell membranes (PSMA positive) were investigated using a N-acetylated-α-linked acidic dipeptidase (NAALDase) assay and revealed high receptor binding affinity for the [DUPA-6-Ahx-(^{nat}Cu-NODAGA)-5-Ava-BBN(7–14)NH2] conjugate (IC_{50} = 1.16 ±1.35 nM) [4].GRPR binding in PC3 cells was evaluated via competitive displacement binding assays and showed an IC_{50} of 3.09 ± 0.34 nM. Subsequently, biodistribution analyses in PC-3 xenografted SCID mice were conducted demonstrating predominate renal clearance, and notable retention of the radioligand in the liver, spleen, small intestine, and PSMA-positive kidney. Larger molecular size and hydrophobic properties may have contributed to this uptake and subsequent retention of tracer. The substantial accumulation

and retention of the tracer in the gut limits the ability of [DUPA-6-Ahx-(^{64}Cu-NODAGA)-5-Ava-BBN(7–14)NH_2] to target primary and metastatic lower abdominal disease. The PET images acquired for [DUPA-6-Ahx-(^{64}Cu-NODAGA)-5-Ava-BBN (7–14)NH2] in PC-3 (GRPR-positive) and LNCaP (PSMA-positive) PCa cells did not exhibit greater performance when compared to analogous monovalent counterparts [4].

As a result of these studies, this same research team moved forward to create an alternative PSMA-BBN agent to decrease background activity in collateral organs by changing from agonist BBN(7–14)NH_2 to an antagonist GRPR-targeting moiety. Work by Bandari et al. Progressed further in the enhancement of a superior dual-biomarker targeting ligand, [DUPA-6-Ahx-Lys(DOTA)-6-Ahx-RM2], as part of their ongoing development efforts (Figure 16). This targeting agent maintained the urea based PSMA targeting motif and modified the GRPR motif to the antagonist RM2. Following synthesis and characterization of [DUPA-6-Ahx-Lys(DOTA)-6-Ahx-RM2], the bivalent agent was metalated with $^{nat/67}GaCl_3$, $^{nat/111}InCl_3$, and $^{nat/177}LuCl_3$ with high radiochemical purity and yield (≥95%). Competitive displacement assays with LNCaP and PC-3 human cancer cell lines demonstrated high binding affinities for PSMA and GRPR of 9.30 ± 2.32 nM and 3.99 ± 1.8 nM, respectively [135]. The 6-aminohexanoic acid pharmacokinetic modifier was substituted with 8-aminooctanoic acid to form the novel [DUPA-6-Ahx-Lys (DOTA)-8-Aoc-RM2]. Thereafter, the bivalent species was metalated in high radiochemical yield (≥98%) with $^{nat/111}InCl_3$ for SPECT imaging and $^{nat/177}LuCl_3$ for possible TRT [3]. This compound showed improved pharmacokinetic and biodistribution results in comparison to the first-generation radiotracer. At 1 h p.i., accumulation of [DUPA-6-Ahx-Lys(^{177}Lu-DOTA)-8-Aoc-RM2] in PC3 and PC3-PIP xenografted mice were 7.51 ± 2.61 and 7.37 ± 2.89%ID/g, respectively. The ^{111}In labeled conjugate had uptake values of 4.74 ± 0.90%ID/g in PC3 tumors and 5.38 ± 1.07%ID/g in PC3-PIP tumors. Single-photon emission tomography/CT investigations at 4 h p.i. showed no uptake in collateral tissues other than kidney, with high uptake and retention in tumors [3]. A blocking investigation was completed to validate the multivalent nature of the tracers. Mice bearing bilateral PSMA- and GRPR-expressing PC3-PIP and GRPR-expressing PC3 tumors were administered a blocking agent of either 2-PMPA or BBN(1–14) peptide as well as a total block administering both agents 15 min prior to the injection of the radiotracer (Figure 17).

The research team at the National Autonomous University of Mexico have evaluated their own BBN/PSMA-targeting bivalent radiotracer with the BBN agonist Lys^3-BN in efforts to decrease radiotracer uptake in benign tissues as demonstrated previously [131]. The ^{68}Ga radiolabeled bivalent, Glu-CO-Lys[2Nal-Cys [Lys^3(GMBS)-BBN-NH_2]-DOTA] (denoted iPSMA-BN), demonstrated high stability in human serum up to 3 h and greater cell uptake and internalization in both PC3 and LNCaP cells in comparison to ^{68}Ga-iPSMA or ^{68}Ga-BN. Pharmacokinetic properties showed PSMA mediated high spleen and renal uptake with rapid excretion via the renal-urinary system. Preclinical imaging done with PC3 and GRPR expressing tumors in the lungs of nude mice demonstrated favorable uptake in PCa lesions [131]. This agent was subsequently administered intravenously to four healthy volunteers (2 male, 2 female) to determine the biokinetics and dosimetry in human patients [132]. The blood clearance was rapid at $T_{1/2}$ = 2.64 min in comparison to the monomer ^{68}Ga-iPSMA ($T_{1/2}$ = 6.5 min in the blood). The internal iliac nodes were clearly visualized

(SUV_{max} = 4.7) due to targeted radiotracer accumulation. However, the monovalent species ^{68}Ga-iPSMA showed a higher SUV_{max} than the^{68}Ga-iPSMA-BN heterodimer in the same tissue [132].

The PSMA/GRPR specific heterodimer, NOTA-DUPA-RM26, prepared by Mitran et al. [133] has been synthesized and radiolabeled using both ^{111}In and ^{68}Ga.This bivalent radioligand displayed high stability and favorable specific binding affinity to PSMA and GRPR in vitro. This was demonstrated through experiments using PSMA-expressing LNCaP cells, GRPR-expressing PC3 cells, and dual expressing PC3-PIP cells. Furthermore, the in vivo imaging outcomes revealed only partial blockage of the radiotracer at 1 h p.i., using PSMA-617 or NOTA-PEG6-RM26 as the blocking agents in PC3-PIP xeno-grafted tumor models [133].

Bailly et al. [136] have investigated a new heterodimer specific for PSMA and GRPR in the context of creating heterobivalent ligands through a simplified “one-pot” synthetic approach. This strategy seeks to mitigate the challenges associated with the arduous production of intricate dual-targeting molecules. The modular synthesis process can be accomplished within less than 24 h, utilizing a molecular scaffold with reactive 3,6-dichloro-1,2,4,5-tetrazine as the initial material and suitable partners for sequential nucleophilic aromatic substitution and inverse electron-demand Diels-Alder reactions. This reaction effectively increases the distance between the two targeting moieties from the dichlorotetrazine platform, a crucial aspect for optimizing the advantages of ligand heterobivalency. The two targeting moieties in this synthesis were the low molecular weight PSMA-targeting urea-based inhibitor KuE (lysine-urea-glutamate) and the GRPR-targeting antagonist JMV594. Evaluation of the pharmacologic properties of the 68Ga labeled radio-conjugate through in vivo and in vitro studies demonstrated that the platform-based assembly method does not hinder the interaction of the ligands with their receptors [136].

4 | CONCLUSION

The field of personalized nuclear medicine is currently undergoing a transformative shift due to the introduction of multimeric peptide-based radiopharmaceuticals. Although considerable progress has been achieved in recent years by conventional techniques involving monovalent bioactive peptides, nanoparticles, or antibodies, researchers are increasingly embracing a heterobivalent strategy to enhance the radiotracer’s pharmacological properties and theranostic potential. As the scientific community shifts toward heterobivalent approaches, greater leaps will be made in new drug delivery systems in the fight against cancer. Advances in radiochemistry and chelation chemistry have further allowed precise tuning of these peptides for radiolabeling with various radionuclides, catering to a wide array of medical applications within nuclear oncology. As research continues to evolve, these insights pave the way for the continued development and implementation of innovative radiopharmaceuticals into the clinical arena.

While traditional monovalent approaches have continued commendable achievements, they lack the ability to face limitations with the intricate, heterogeneous nature of tumors. Not all cancers are the same and can vary in type and amount depending on the individual

patient or the stage of cancer. The bivalent radiotracers described herein provide substantial evidence in displaying the advantages of amalgamating the dual receptor-targeting actions of emerging theranostic radiopharmaceuticals. While the synthesis of heterobivalent ligands is acknowledged for its complexity and time-consuming nature, streamlined methods of synthesis are ongoing expedite the difficult process. It is believed the potential benefits of these radiopharmaceuticals outweigh the inherent challenges associated with their synthesis. By utilizing a single agent to target multiple known biomarkers, the potential impact encompasses broader patient coverage, precise staging, customized treatment design, and the potential for improved patient outcomes and quality of life.

In conclusion, employing bivalency to engage multiple targets simultaneously holds the potential to surpass the capabilities of monovalent peptide-based radiopharmaceuticals. As the scientific community gradually embraces the usage for heterobivalent approaches, successful strategies to effectively combat cancer across diverse patient profiles and varying cancer stages will be developed. Harnessing the combined potential between multiple targeting strategies, these approaches could unlock new dimensions of accuracy, sensitivity, and specificity of disease.

Funding information

NIH Research Evaluation and Commercilization Hub, Grant/Award Number: 1U01HL152410; USVA Medical Research Service, Grant/Award Number: I01 BX00096409; National Institutes of Health, Grant/Award Numbers: R01CA269221, R01CA225837

DATA AVAILABILITY STATEMENT

There is no data for this review.

Abbreviations:

α	alpha
α-MSH	α-Melanocyte-Stimulating Hormone
β^-	beta
β^+	positron
γ	gamma
BBN	bombesin peptide
BFCA	bifunctional chelating agent
GRPR	gastrin-releasing peptide receptors
MC1R	melanocortin 1 receptor
NE	neuroendocrine
NEC	neuroendocrine carcinoma

NET	neuroendocrine tumors
p.i.	post-intravenous injection
PCa	prostate cancer
PEG	polyethylene glycol
PET	positron emission tomography
PRRT	peptide receptor radionuclide therapy
PSMA	prostate specific membrane antigen
RAFT	regioselective addressable functionalized template
SPECT	single photon emission computed tomography
SST	somatostatin
TRT	targeted radionuclide therapy

REFERENCES

[1]. Behr T, Gotthardt M, Barth A, Behe M. Imaging tumors with peptide-based radioligands. Q J Nucl Med Mol Imag. 2001;45:189.

[2]. Okarvi SM, Maecke HR. Peptides for nuclear medicine therapy: chemical properties and production; 2013.

[3]. Bandari RP, Carmack TL, Malhotra A, Watkinson L, Fergason Cantrell EA, Lewis MR, et al. Development of heterobivalent theranostic probes having high affinity/selectivity for the GRPR/PSMA. J Med Chem. 2021;64(4):2151–66. 10.1021/acs.jmedchem.0c01785 [PubMed: 33534560]

[4]. Bandari RP, Jiang Z, Reynolds TS, Bernskoetter NE, Szczodroski AF, Bassuner KJ, et al. Synthesis and biological evaluation of copper-64 radiolabeled [DUPA-6-Ahx-(NODAGA)-5-Ava-BBN(7–14)NH2], a novel bivalent targeting vector having affinity for two distinct biomarkers (GRPr/PSMA) of prostate cancer. Nucl Med Biol. 2014;41(4):355–63. 10.1016/j.nucmedbio.2014.01.001 [PubMed: 24508213]

[5]. Durkan K, Jiang Z, Rold TL, Sieckman GL, Hoffman TJ, Bandari RP, et al. A heterodimeric [RGD-Glu-[^{64}Cu-NO2A]-6-Ahx-RM2] αvβ3/GRPr-targeting antagonist radiotracer for PET imaging of prostate tumors. Nucl Med Biol. 2014;41(2): 133–9. 10.1016/j.nucmedbio.2013.11.006 [PubMed: 24480266]

[6]. Judmann B, Braun D, Wängler B, Schirrmacher R, Fricker G, Wängler C. Current state of radiolabeled heterobivalent peptidic ligands in tumor imaging and therapy. Pharmaceuticals. 2020;13(8):173. 10.3390/ph13080173 [PubMed: 32751666]

[7]. Fischer G, Schirrmacher R, Wängler B, Wängler C. Radiolabeled heterobivalent peptidic ligands: an approach with high future potential for in vivo imaging and therapy of malignant diseases. ChemMedChem. 2013;8(6):883–90. 10.1002/cmdc.201300081 [PubMed: 23564566]

[8]. Chen X, Liu S, Hou Y, Tohme M, Park R, Bading JR, et al. MicroPET imaging of breast cancer αv-integrin expression with ^{64}Cu-labeled dimeric RGD peptides. Mol Imag Biol. 2004;6(5):350–9. 10.1016/j.mibio.2004.06.004

[9]. Dijkgraaf I, Kruijtzer JA, Liu S, Soede AC, Oyen WJ, Corstens FH, et al. Improved targeting of the $\alpha_v\beta_3$ integrin by multi-merisation of RGD peptides. Eur J Nucl Med Mol Imag. 2007;34(2):267–73. 10.1007/s00259-006-0180-9

[10]. Dijkgraaf I, Yim CB, Franssen GM, Schuit RC, Luurtsema G, Liu S, et al. PET imaging of $\alpha v\beta_3$ integrin expression in tumours with ^{68}Ga-labelled mono-di-and tetrameric RGD peptides. Eur J Nucl Med Mol Imag. 2011;38(1):128–37. 10.1007/s00259-010-1615-x

[11]. Liu S Radiolabeled cyclic RGD peptides as integrin alpha(v) beta(3)-targeted radiotracers: maximizing binding affinity via bivalency. Bioconjug Chem. 2009;20(12):2199–213. 10.1021/bc900167c [PubMed: 19719118]

[12]. Nhàn NTT, Yamada T, Yamada KH. Peptide-based agents for cancer treatment: current applications and future directions. Int J Mol Sci. 2023:24.

[13]. Cheetham AG, Keith D, Zhang P, Lin R, Su H, Cui H. Targeting tumors with small molecule peptides. Curr Cancer Drug Targets. 2016;16(6):489–508. 10.2174/1568009616666151130214646 [PubMed: 26632435]

[14]. Pruis IJ, Van Dongen GAMS, Veldhuijzen Van Zanten SEM. The added value of diagnostic and theranostic PET imaging for the treatment of CNS tumors. Int J Mol Sci. 2020;21(3): 1029. 10.3390/ijms21031029 [PubMed: 32033160]

[15]. Jamous M, Haberkorn U, Mier W. Synthesis of peptide radiopharmaceuticals for the therapy and diagnosis of tumor diseases. Molecules. 2013;18(3):3379–409. 10.3390/molecules18033379 [PubMed: 23493103]

[16]. Fisher R, Pusztai L, Swanton C. Cancer heterogeneity: implications for targeted therapeutics. Br J Cancer. 2013;108(3): 479–85. 10.1038/bjc.2012.581 [PubMed: 23299535]

[17]. Sarhadi VK, Armengol G. Molecular biomarkers in cancer. Biomolecules. 2022;12(8):1021. 10.3390/biom12081021 [PubMed: 35892331]

[18]. Ambrosini V, Kunikowska J, Baudin E, Bodei L, Bouvier C, Capdevila J, et al. Consensus on molecular imaging and theranostics in neuroendocrine neoplasms. Eur J Cancer. 2021;146:56–73. 10.1016/j.ejca.2021.01.008 [PubMed: 33588146]

[19]. Hicks RJ, Kwekkeboom DJ, Krenning E, Bodei L, Grozinsky-Glasberg S, Arnold R, et al. ENETS consensus guidelines for the standards of care in neuroendocrine neoplasms: peptide receptor radionuclide therapy with radiolabelled somatostatin analogues. Neuroendocrinology. 2017;105(3):295–309. 10.1159/000475526 [PubMed: 28402980]

[20]. Shah MH, Goldner WS, Benson AB, Bergsland E, Blaszkowsky LS, Brock P, et al. Neuroendocrine and adrenal tumors, version 2.2021, NCCN clinical practice guidelines in oncology. J Natl Compr Canc Netw. 2021;19(7):839–68. 10.6004/jnccn.2021.0032 [PubMed: 34340212]

[21]. Veber DF, Freidinger RM, Perlow DS, Paleveda WJ, Holly FW, Strachan RG, et al. A potent cyclic hexapeptide analogue of somatostatin. Nature. 1981;292(5818):55–8. 10.1038/292055a0 [PubMed: 6116194]

[22]. Veber DF, Holly FW, Nutt RF, Bergstrand SJ, Brady SF, Hisrschmann R, et al. Highly active cyclic and bicyclic somatostatin analogues of reduced ring size. Nature. 1979;280(5722):512–4. 10.1038/280512a0 [PubMed: 460433]

[23]. Bauer W, Briner U, Doepfner W, Haller R, Huguenin R, Marbach P, et al. Sms 201–995: a very potent and selective octapeptide analogue of somatostatin with prolonged action. Life Sci. 1982;31(11):1133–40. 10.1016/0024-3205(82)90087-x [PubMed: 6128648]

[24]. Krenning E, Koolj P, Bakker W, Breeman W, Postema P, Kwekkeboom DJ, et al. Radiotherapy with a radiolabeled somatostatin analogue,[^{111}In-DTPA-D-Phe1]-octreotide. A case history. New York Academy of Sciences. Annals 1994; 733(1):496–506. 10.1111/j.1749-6632.1994.tb17300.x

[25]. Krenning EP, Breeman WA, Kooij PP, Lameris J, Bakker WH, Koper J, et al. Localisation of endocrine-related tumours with radioiodinated analogue of somatostatin. Lancet. 1989;333(8632):242–4. 10.1016/s0140-6736(89)91258-0

[26]. Hofman MS, Michael M, Hicks RJ. ^{177}Lu-Dotatate for midgut neuroendocrine tumors. N Engl J Med. 2017;376:1390–1.

[27]. Strosberg J, Wolin E, Chasen B, Kulke M, Bushnell D, Caplin M, et al. Health-related quality of life in patients with progressive midgut neuroendocrine tumors treated with ^{177}Lu-Dotatate in the phase III NETTER-1 trial. J Clin Oncol. 2018;36(25):2578–84. 10.1200/jco.2018.78.5865 [PubMed: 29878866]

[28]. Kwekkeboom DJ, Kam BL, van Essen M, Teunissen JJ, van Eijck CH, Valkema R, et al. Somatostatin-receptor-based imaging and therapy of gastroenteropancreatic neuroendocrine tumors. Endocr Relat Cancer. 2010;17(1):R53–73. 10.1677/erc-09-0078 [PubMed: 19995807]

[29]. Ginj M, Schmitt JS, Chen J, Waser B, Reubi JC, de Jong M, et al. Design, synthesis, and biological evaluation of somatostatin-based radiopeptides. Chem Biol. 2006;13(10): 1081–90. 10.1016/j.chembiol.2006.08.012 [PubMed: 17052612]

[30]. Chen Y, Dhara S, Banerjee SR, Byun Y, Pullambhatla M, Mease RC, et al. A low molecular weight PSMA-based fluorescent imaging agent for cancer. Biochem Biophys Res Commun. 2009;390(3):624–9. 10.1016/j.bbrc.2009.10.017 [PubMed: 19818734]

[31]. Silver DA, Pellicer I, Fair WR, Heston WD, Cordon-Cardo C. Prostate-specific membrane antigen expression in normal and malignant human tissues. Clin Cancer Res. 1997;3:81–5. [PubMed: 9815541]

[32]. Wright GL Jr., Grob BM, Haley C, Grossman K, Newhall K, Petrylak D, et al. Upregulation of prostate-specific membrane antigen after androgen-deprivation therapy. Urology. 1996;48(2):326–34. 10.1016/s0090-4295(96)00184-7 [PubMed: 8753752]

[33]. Fernández R, Soza-Ried C, Iagaru A, Stephens A, Müller A, Schieferstein H, et al. Imaging GRPr expression in meta-static castration-resistant prostate cancer with [^{68}Ga]Ga-RM2-A head-to-head pilot comparison with [^{68}Ga]Ga-PSMA-11. Cancers. 2023;16(1):173. 10.3390/cancers16010173 [PubMed: 38201600]

[34]. Wynant GE, Murphy GP, Horoszewicz JS, Neal CE, Collier BD, Mitchell E, et al. Immunoscintigraphy of prostatic cancer: preliminary results with 111In-labeled monoclonal antibody 7E11-C5.3 (CYT-356). Prostate. 1991;18(3):229–41. 10.1002/pros.2990180305 [PubMed: 2020619]

[35]. Osborne JR, Akhtar NH, Vallabhajosula S, Anand A, Deh K, Tagawa ST. Prostate-specific membrane antigen-based imaging. Urol Oncol. 2013;31(2):144–54. 10.1016/j.urolonc.2012.04.016 [PubMed: 22658884]

[36]. Mease RC, Foss CA, Pomper MG. PET imaging in prostate cancer: focus on prostate-specific membrane antigen. Curr Top Med Chem. 2013;13(8):951–62. 10.2174/1568026611313080008 [PubMed: 23590171]

[37]. Hennrich U, Eder M. [^{68}Ga]Ga-PSMA-11: the first FDA-approved 68Ga-radiopharmaceutical for PET imaging of prostate cancer. Pharmaceuticals. 2021;14(8):713. 10.3390/ph14080713 [PubMed: 34451810]

[38]. Afshar-Oromieh A, Hetzheim H, Kübler W, Kratochwil C, Giesel FL, Hope TA, et al. Radiation dosimetry of ^{68}Ga-PSMA-11 (HBED-CC) and preliminary evaluation of optimal imaging timing. Eur J Nucl Med Mol Imag. 2016; 43(9):1611–20. 10.1007/s00259-016-3419-0

[39]. Hennrich U, Eder M. [^{177}Lu]Lu-PSMA-617 (Pluvicto(TM)): the first FDA-approved radiotherapeutical for treatment of prostate cancer. Pharmaceuticals. 2022;15(10):1292. 10.3390/ph15101292 [PubMed: 36297404]

[40]. Emmett L, Crumbaker M, Ho B, Willowson K, Eu P, Ratnayake L, et al. Results of a prospective phase 2 pilot trial of ^{177}Lu–PSMA-617 therapy for metastatic castration-resistant prostate cancer including imaging predictors of treatment response and patterns of progression. Clin Genitourin Cancer. 2019;17(1):15–22. 10.1016/j.clgc.2018.09.014 [PubMed: 30425003]

[41]. Jones W, Griffiths K, Barata PC, Paller CJ. PSMA theranostics: review of the current status of PSMA-targeted imaging and radioligand therapy. Cancers. 2020;12(6):1367. 10.3390/cancers12061367 [PubMed: 32466595]

[42]. Ruigrok EA, van Weerden WM, Nonnekens J, de Jong M. The future of PSMA-targeted radionuclide therapy: an overview of recent preclinical research. Pharmaceutics. 2019; 11:560. 10.3390/pharmaceutics11110560 [PubMed: 31671763]

[43]. Niaz MJ, Sun M, Skafida M, Niaz MO, Ivanidze J, Osborne JR, et al. Review of commonly used prostate specific PET tracers used in prostate cancer imaging in current clinical practice. Clin Imag. 2021;79:278–88. 10.1016/j.clinimag.2021.06.006

[44]. Jensen RT, Battey JF, Spindel ER, Benya RV. International Union of Pharmacology. LXVIII. Mammalian bombesin receptors: nomenclature, distribution, pharmacology, signaling, and

functions in normal and disease states. Pharmacol Rev. 2008;60:1–42. 10.1124/pr.107.07108 [PubMed: 18055507]

[45]. Mansi R, Fleischmann A, Mäcke HR, Reubi JC. Targeting GRPR in urological cancers—from basic research to clinical application. Nat Rev Urol. 2013;10(4):235–44. 10.1038/nrurol.2013.42 [PubMed: 23507930]

[46]. Nagasaki S, Nakamura Y, Maekawa T, Akahira J, Miki Y, Suzuki T, et al. Immunohistochemical analysis of gastrin-releasing peptide receptor (GRPR) and possible regulation by estrogen receptor βcx in human prostate carcinoma. Neoplasma. 2012;59(02):224–32. 10.4149/neo_2012_029 [PubMed: 22248281]

[47]. Sun B, Halmos G, Schally AV, Wang X, Martinez M. Presence of receptors for bombesin/gastrin-releasing peptide and mRNA for three receptor subtypes in human prostate cancers. Prostate. 2000;42(4):295–303. 10.1002/(sici)1097-0045(20000301)42:4<295::aid-pros7>3.3.co;2-2 [PubMed: 10679759]

[48]. Markwalder R, Reubi JC. Gastrin-releasing peptide receptors in the human prostate: relation to neoplastic transformation. Cancer Res. 1999;59:1152–9. [PubMed: 10070977]

[49]. Fleischmann A, Waser B, Reubi JC. High expression of gastrin-releasing peptide receptors in the vascular bed of urinary tract cancers: promising candidates for vascular targeting applications. Endocr Relat Cancer. 2009;16(2):623–33. 10.1677/erc-08-0316 [PubMed: 19478282]

[50]. Beer M, Montani M, Gerhardt J, Wild PJ, Hany TF, Hermanns T, et al. Profiling gastrin-releasing peptide receptor in prostate tissues: clinical implications and molecular correlates. Prostate. 2012;72(3):318–25. 10.1002/pros.21434 [PubMed: 21739464]

[51]. Baratto L, Jadvar H, Iagaru A. Prostate cancer theranostics targeting gastrin-releasing peptide receptors. Mol Imag Biol. 2018;20(4):501–9. 10.1007/s11307-017-1151-1

[52]. Mansi R, Nock BA, Dalm SU, Busstra MB, van Weerden WM, Maina T. Radiolabeled bombesin analogs. Cancers. 2021;13(22):5766. 10.3390/cancers13225766 [PubMed: 34830920]

[53]. Baum RP, Prasad V, Mutloka N. Molecular imaging of bombesin receptors in various tumors by Ga-68 AMBA PET/CT: first results. J Nucl Med. 2007;48:79P.

[54]. Mansi R, Wang X, Forrer F, Kneifel S, Tamma ML, Waser B, et al. Evaluation of a 1,4,7,10-tetraazacyclododecane-1,4,7,10-tetraacetic acid-conjugated bombesin-based radio-antagonist for the labeling with single-photon emission computed tomography, positron emission tomography, and therapeutic radionuclides. Clin Cancer Res. 2009;15(16): 5240–9. 10.1158/1078-0432.ccr-08-3145 [PubMed: 19671861]

[55]. Thomas R, Chen J, Roudier M, Vessella R, Lantry L, Nunn A. In vitro binding evaluation of ^{177}Lu-AMBA, a novel ^{177}Lu-labeled GRP-R agonist for systemic radiotherapy in human tissues. Clin Exp Metastasis. 2008;26(2):105–19. 10.1007/s10585-008-9220-0 [PubMed: 18975117]

[56]. Prasanphanich AF, Retzloff L, Lane SR, Nanda PK, Sieckman GL, Rold TL, et al. In vitro and in vivo analysis of [^{64}Cu-NO2A-8-Aoc-BBN(7–14)NH(2)]: a site-directed radiopharmaceutical for positron-emission tomography imaging of T-47D human breast cancer tumors. Nucl Med Biol. 2009; 36(2):171–81. 10.1016/j.nucmedbio.2008.11.005 [PubMed: 19217529]

[57]. Carlucci G, Kuipers A, Ananias HJ, de Paula Faria D, Dierckx RA, Helfrich W, et al. GRPR-selective PET imaging of prostate cancer using [^{18}F]-lanthionine-bombesin analogs. Peptides. 2015;67:45–54. 10.1016/j.peptides.2015.03.004 [PubMed: 25797109]

[58]. Lane SR, Nanda P, Rold TL, Sieckman GL, Figueroa SD, Hoffman TJ, et al. Optimization, biological evaluation and microPET imaging of copper-64-labeled bombesin agonists, [^{64}Cu-NO2A-(X)-BBN(7–14)NH2], in a prostate tumor xenografted mouse model. Nucl Med Biol. 2010;37(7):751–61. 10.1016/j.nucmedbio.2010.04.016 [PubMed: 20870150]

[59]. de Castiglione R, Gozzini L. Bombesin receptor antagonists. Crit Rev Oncol-Hematol. 1996;24(2):117–51. 10.1016/1040-8428(96)00220-x [PubMed: 8889369]

[60]. Wieser G, Popp I, Christian Rischke H, Drendel V, Grosu A-L, Bartholomä M, et al. Diagnosis of recurrent prostate cancer with PET/CT imaging using the gastrin-releasing peptide receptor antagonist ^{68}Ga-RM2: preliminary results in patients with negative or inconclusive [^{18}F] Fluoroethylcho-line-PET/CT. Eur J Nucl Med Mol Imag. 2017;44(9):1463–72. 10.1007/s00259-017-3702-8

[61]. Minamimoto R, Sonni I, Hancock S, Vasanawala S, Loening A, Gambhir SS, et al. Prospective evaluation of ^{68}Ga-RM2 PET/MRI in patients with biochemical recurrence of prostate cancer and negative findings on conventional imaging. J Nucl Med. 2018;59(5):803–8. 10.2967/jnumed.117.197624 [PubMed: 29084827]

[62]. Kurth J, Krause BJ, Schwarzenböck SM, Bergner C, Hakenberg OW, Heuschkel M. First-in-human dosimetry of gastrin-releasing peptide receptor antagonist [^{177}Lu]Lu-RM2: a radiopharmaceutical for the treatment of metastatic castration-resistant prostate cancer. Eur J Nucl Med Mol Imag. 2020;47(1):123–35. 10.1007/s00259-019-04504-3

[63]. Baratto L, Jadvar H, Iagaru A. Prostate cancer theranostics targeting gastrin-releasing peptide receptors. Mol Imag Biol. 2018;20(4):501–9. 10.1007/s11307-017-1151-1

[64]. Valdembri D, Serini G. The roles of integrins in cancer. Fac Rev. 2021;10:45. 10.12703/r/10-45 [PubMed: 34131655]

[65]. Weis SM, Cheresh DA. αV integrins in angiogenesis and cancer. Cold Spr Harb Perspect Med. 2011;1:a006478. 10.1101/cshperspect.a006478

[66]. Ludwig BS, Kessler H, Kossatz S, Reuning U. RGD-binding integrins revisited: how recently discovered functions and novel synthetic ligands (Re-)Shape an ever-evolving field. Cancers. 2021;13(7):1711. 10.3390/cancers13071711 [PubMed: 33916607]

[67]. Seguin J, Nicolazzi C, Mignet N, Scherman D, Chabot GG. Vascular density and endothelial cell expression of integrin alpha v beta 3 and E-selectin in murine tumours. Tum Biol. 2012;33(5):1709–17. 10.1007/s13277-012-0428-x

[68]. Haubner R, Weber WA, Beer AJ, Vabuliene E, Reim D, Sarbia M, et al. Noninvasive visualization of the activated alphavbeta3 integrin in cancer patients by positron emission tomography and [^{18}F]Galacto-RGD. PLoS Med. 2005;2(3): e70. 10.1371/journal.pmed.0020070 [PubMed: 15783258]

[69]. Zhou Y, Kim YS, Chakraborty S, Shi J, Gao H, Liu S. ^{99m}Tc-labeled cyclic RGD peptides for noninvasive monitoring of tumor integrin $\alpha_v\beta_3$ expression. Mol Imag. 2011;10(5):386–97. 10.2310/7290.2011.00006

[70]. Badipa F, Alirezapour B, Yousefnia H. An overview of radiolabeled RGD peptides for theranostic applications. Curr Rad. 2023;16(2):107–22. 10.2174/1874471016666221207122731

[71]. Kapp TG, Rechenmacher F, Neubauer S, Maltsev OV, Cavalcanti-Adam EA, Zarka R, et al. A comprehensive evaluation of the activity and selectivity profile of ligands for RGD-binding integrins. Sci Rep. 2017;7(1):39805. 10.1038/srep39805 [PubMed: 28074920]

[72]. Ma Y, Ai G, Zhang C, Zhao M, Dong X, Han Z, et al. Novel linear peptides with high affinity to αvβ3 integrin for precise tumor identification. Theranostics. 2017;7(6):1511–23. 10.7150/thno.18401 [PubMed: 28529634]

[73]. Garanger E, Boturyn D, Jin Z, Dumy P, Favrot MC, Coll JL. New multifunctional molecular conjugate vector for targeting, imaging, and therapy of tumors. Mol Ther. 2005;12(6): 1168–75. 10.1016/j.ymthe.2005.06.095 [PubMed: 16051524]

[74]. Boturyn D, Coll JL, Garanger E, Favrot MC, Dumy P. Template assembled cyclopeptides as multimeric system for integrin targeting and endocytosis. J Am Chem Soc. 2004; 126(18):5730–9. 10.1021/ja049926n [PubMed: 15125666]

[75]. Bozon-Petitprin A, Bacot S, Gauchez AS, Ahmadi M, Bourre JC, Marti-Batlle D, et al. Targeted radionuclide therapy with RAFT-RGD radiolabelled with ^{90}Y or ^{177}Lu in a mouse model of $\alpha_v\beta_3$-expressing tumours. Eur J Nucl Med Mol Imag. 2015;42(2):252–63. 10.1007/s00259-014-2891-7

[76]. Jin ZH, Furukawa T, Degardin M, Sugyo A, Tsuji AB, Yamasaki T, et al. $\alpha_v\beta_3$ integrin-targeted radionuclide therapy with ^{64}Cu-cyclam-RAFT-c(-RGDfK-)4. Mol Cancer Ther. 2016;15(9):2076–85. 10.1158/1535-7163.mct-16-0040 [PubMed: 27422811]

[77]. Cossu J, Thoreau F, Boturyn D. Multimeric RGD-based strategies for selective drug delivery to tumor tissues. Pharmaceutics. 2023;15(2):525. 10.3390/pharmaceutics15020525 [PubMed: 36839846]

[78]. Siegrist W, Solca F, Stutz S, Giuffrè L, Carrel S, Girard J, et al. Characterization of receptors for alpha-melanocyte-stimulating hormone on human melanoma cells. Cancer Res. 1989;49:6352–8. [PubMed: 2804981]

[79]. Tatro JB, Wen Z, Entwistle ML, Atkins MB, Smith TJ, Reichlin S, et al. Interaction of an alpha-melanocyte-stimulating hormone-diphtheria toxin fusion protein with melanotropin receptors in human melanoma metastases. Cancer Res. 1992;52:2545–8. [PubMed: 1314697]

[80]. Yang J, Xu J, Gonzalez R, Lindner T, Kratochwil C, Miao Y. 68Ga-DOTA-GGNle-CycMSH$_{hex}$ targets the melanocortin-1 receptor for melanoma imaging. Sci Transl Med. 2018;10(466). 10.1126/scitranslmed.aau4445

[81]. Cheresh DA, Spiro RC. Biosynthetic and functional properties of an Arg-Gly-Asp-directed receptor involved in human melanoma cell attachment to vitronectin, fibrinogen, and von Willebrand factor. J Biol Chem. 1987;262(36):17703–11. 10.1016/s0021-9258(18)45436-1 [PubMed: 2447074]

[82]. Petitclerc E, Strömblad S, von Schalscha TL, Mitjans F, Piulats J, Montgomery AM, et al. Integrin alpha(v)beta3 promotes M21 melanoma growth in human skin by regulating tumor cell survival. Cancer Res. 1999;59:2724–30. [PubMed: 10363998]

[83]. Albelda SM, Mette SA, Elder DE, Stewart R, Damjanovich L, Herlyn M, et al. Integrin distribution in malignant melanoma: association of the beta 3 subunit with tumor progression. Cancer Res. 1990;50:6757–64. [PubMed: 2208139]

[84]. Miao Y, Benwell K, Quinn TP. ^{99m}Tc- and ^{111}In-labeled alpha-melanocyte-stimulating hormone peptides as imaging probes for primary and pulmonary metastatic melanoma detection. J Nucl Med. 2007;48:73–80. [PubMed: 17204701]

[85]. Guo H, Yang J, Gallazzi F, Miao Y. Reduction of the ring size of radiolabeled lactam bridge-cyclized alpha-MSH peptide, resulting in enhanced melanoma uptake. J Nucl Med. 2010; 51(3):418–26. 10.2967/jnumed.109.071787 [PubMed: 20150256]

[86]. Guo H, Yang J, Gallazzi F, Miao Y. Effects of the amino acid linkers on the melanoma-targeting and pharmacokinetic properties of 111In-labeled lactam bridge-cyclized alpha-MSH peptides. J Nucl Med. 2011;52(4):608–16. 10.2967/jnumed.110.086009 [PubMed: 21421725]

[87]. Guo H, Miao Y. Cu-64-labeled lactam bridge-cyclized α-MSH peptides for PET imaging of melanoma. Mol Pharm. 2012;9(8):2322–30. 10.1021/mp300246j [PubMed: 22780870]

[88]. Guo H, Miao Y. Introduction of an 8-aminooctanoic acid linker enhances uptake of ^{99m}Tc-labeled lactam bridge-cyclized α-MSH peptide in melanoma. J Nucl Med. 2014; 55(12):2057–63. 10.2967/jnumed.114.145896 [PubMed: 25453052]

[89]. Yang J, Xu J, Cheuy L, Gonzalez R, Fisher DR, Miao Y. Evaluation of a novel Pb-203-Labeled lactam-cyclized alpha-melanocyte-stimulating hormone peptide for melanoma targeting. Mol Pharm. 2019;16(4):1694–702. 10.1021/acs.molpharmaceut.9b00025 [PubMed: 30763112]

[90]. Qiao Z, Xu J, Gonzalez R, Miao Y. Novel [^{99m}Tc]-Tricarbonyl-NOTA-Conjugated lactam-cyclized alpha-MSH peptide with enhanced melanoma uptake and reduced renal uptake. Mol Pharm. 2020;17(9):3581–8. 10.1021/acs.molpharmaceut.0c00606 [PubMed: 32663011]

[91]. Miao Y, Quinn TP. Advances in receptor-targeted radiolabeled peptides for melanoma imaging and therapy. J Nucl Med. 2021;62(3):313–8. 10.2967/jnumed.120.243840 [PubMed: 33277401]

[92]. Qiao Z, Xu J, Fisher DR, Gonzalez R, Miao Y. Introduction of a polyethylene glycol linker improves uptake of ^{67}Cu-NOTA-Conjugated lactam-cyclized alpha-melanocyte-stimulating hormone peptide in melanoma. Cancers. 2023;15(10):2755. 10.3390/cancers15102755 [PubMed: 37345092]

[93]. Liu Z, Niu G, Wang F, Chen X. ^{68}Ga-labeled NOTA-RGD-BBN peptide for dual integrin and GRPR-targeted tumor imaging. Eur J Nucl Med Mol Imag. 2009;36(9):1483–94. 10.1007/s00259-009-1123-z

[94]. Jiang L, Miao Z, Liu H, Ren G, Bao A, Cutler CS, et al. ^{177}Lu-labeled RGD-BBN heterodimeric peptide for targeting prostate carcinoma. Nucl Med Commun. 2013;34(9):909–14. 10.1097/mnm.0b013e328362d2b6 [PubMed: 23708872]

[95]. Jackson AB, Nanda PK, Rold TL, Sieckman GL, Szczodroski AF, Hoffman TJ, et al. ^{64}Cu-NO2A-RGD-Glu-6-Ahx-BBN(7–14)NH2: a heterodimeric targeting vector for positron emission tomography imaging of prostate cancer. Nucl Med Biol. 2012;39(3):377–87. 10.1016/j.nucmedbio.2011.10.004 [PubMed: 22226021]

[96]. Stott Reynolds TJ, Schehr R, Liu D, Xu J, Miao Y, Hoffman TJ, et al. Characterization and evaluation of DOTA-conjugated Bombesin/RGD-antagonists for prostate cancer tumor imaging

and therapy. Nucl Med Biol. 2015;42(2):99–108. 10.1016/j.nucmedbio.2014.10.002 [PubMed: 25459113]

[97]. Liu Z, Yan Y, Liu S, Wang F, Chen X. ^{18}F, ^{64}Cu, and ^{68}Ga labeled RGD-bombesin heterodimeric peptides for PET imaging of breast cancer. Bioconjugate Chem. 2009;20(5): 1016–25. 10.1021/bc9000245

[98]. Liu Z, Yan Y, Chin FT, Wang F, Chen X. Dual integrin and gastrin-releasing peptide receptor targeted tumor imaging using ^{18}F-labeled PEGylated RGD-bombesin heterodimer ^{18}F-FB-PEG$_3$-Glu-RGD-BBN. J Med Chem. 2009;52:425–32. [PubMed: 19113865]

[99]. Li Z-B, Wu Z, Chen K, Ryu EK, Chen X. ^{18}F-labeled BBN-RGD heterodimer for prostate cancer imaging. J Nucl Med. 2008;49:453–61. [PubMed: 18287274]

[100]. Li ZB, Wu Z, Chen K, Ryu EK, Chen X. ^{18}F-labeled BBN-RGD heterodimer for prostate cancer imaging. J Nucl Med. 2008;49(3):453–61. 10.2967/jnumed.107.048009 [PubMed: 18287274]

[101]. Liu Z, Yan Y, Chin FT, Wang F, Chen X. Dual integrin and gastrin-releasing peptide receptor targeted tumor imaging using ^{18}F-labeled PEGylated RGD-bombesin heterodimer ^{18}F-FB-PEG3-Glu-RGD-BBN. J Med Chem. 2009;52(2):425–32. 10.1021/jm801285t [PubMed: 19113865]

[102]. Liu Z, Li ZB, Cao Q, Liu S, Wang F, Chen X. Small-animal PET of tumors with ^{64}Cu-labeled RGD-bombesin heterodimer. J Nucl Med. 2009;50(7):1168–77. 10.2967/jnumed.108.061739 [PubMed: 19525469]

[103]. Liu Z, Niu G, Wang F, Chen X. ^{68}Ga-labeled NOTA-RGD-BBN peptide for dual integrin and GRPR-targeted tumor imaging. Eur J Nucl Med Mol Imag. 2009;36(9):1483–94. 10.1007/s00259-009-1123-z

[104]. Wu Y, Zhang X, Xiong Z, Cheng Z, Fisher DR, Liu S, et al. microPET imaging of glioma integrin $\alpha_v\beta_3$ expression using (64)Cu-labeled tetrameric RGD peptide. J Nucl Med. 2005;46:1707–18. [PubMed: 16204722]

[105]. Jiang Z, Bandari RP, Reynolds TJS, Xu J, Miao Y, Rold TL, et al. Molecular imaging investigations of a 67Ga/^{64}Cu labeled bivalent ligand, [RGD-Glu-(DO3A)-6-Ahx-RM2], targeting GRPR/$\alpha_v\beta_3$ biomarkers: a comparative study. Radiochim Acta. 2016;104(7):499–512. 10.1515/ract-2015-2519

[106]. Siegel RL, Miller KD, Wagle NS, Jemal A. Cancer statistics, 2023. CA Cancer J Clin. 2023;73(1):17–48. 10.3322/caac.21763 [PubMed: 36633525]

[107]. Poethko T, Schottelius M, Thumshirn G, Hersel U, Herz M, Henriksen G, et al. Two-step methodology for high-yield routine radiohalogenation of peptides: 18F-labeled RGD and octreotide analogs. J Nucl Med. 2004;45:892–902. [PubMed: 15136641]

[108]. Li C, Wang W, Wu Q, Ke S, Houston J, Sevick-Muraca E, et al. Dual optical and nuclear imaging in human melanoma xenografts using a single targeted imaging probe. Nucl Med Biol. 2006;33(3):349–58. 10.1016/j.nucmedbio.2006.01.001 [PubMed: 16631083]

[109]. Decristoforo C, Faintuch-Linkowski B, Rey A, von Guggenberg E, Rupprich M, Hernandez-Gonzales I, et al. [^{99m}Tc] HYNIC-RGD for imaging integrin $\alpha_v\beta_3$ expression. Nucl Med Biol. 2006;33(8):945–52. 10.1016/j.nucmedbio.2006.09.001 [PubMed: 17127166]

[110]. Alves S, Correia JD, Gano L, Rold TL, Prasanphanich A, Haubner R, et al. In vitro and in vivo evaluation of a novel ^{99m}Tc(CO)3-pyrazolyl conjugate of cyclo-(Arg-Gly-Asp-d-Tyr-Lys). Bioconjug Chem. 2007;18(2):530–7. 10.1021/bc060234t [PubMed: 17373771]

[111]. Decristoforo C, Hernandez Gonzalez I, Carlsen J, Rupprich M, Huisman M, Virgolini I, et al. ^{68}Ga- and ^{111}In-labelled DOTA-RGD peptides for imaging of $\alpha_v\beta_3$ integrin expression. Eur J Nucl Med Mol Imag. 2008;35(8):1507–15. 10.1007/s00259-008-0757-6

[112]. Hultsch C, Schottelius M, Auernheimer J, Alke A, Wester HJ. 18F-Fluoroglucosylation of peptides, exemplified on cyclo(RGDfK). Eur J Nucl Med Mol Imag. 2009;36(9):1469–74. 10.1007/s00259-009-1122-0

[113]. Yang J, Guo H, Gallazzi F, Berwick M, Padilla RS, Miao Y. Evaluation of a novel Arg-Gly-Asp-conjugated α-melanocyte stimulating hormone hybrid peptide for potential melanoma therapy. Bioconjug Chem. 2009;20(8):1634–42. 10.1021/bc9001954 [PubMed: 19552406]

[114]. Yang J, Guo H, Miao Y. Technetium-99m-labeled Arg-Gly-Asp-conjugated alpha-melanocyte stimulating hormone hybrid peptides for human melanoma imaging. Nucl Med Biol. 2010;37(8):873–83. 10.1016/j.nucmedbio.2010.05.006 [PubMed: 21055617]

[115]. Xu J, Yang J, Miao Y. Dual receptor-targeting ^{99m}Tc-labeled Arg-Gly-Asp-conjugated Alpha-Melanocyte stimulating hormone hybrid peptides for human melanoma imaging. Nucl Med Biol. 2015;42(4):369–74. 10.1016/j.nucmedbio.2014.11.002 [PubMed: 25577037]

[116]. Yang J, Guo H, Padilla RS, Berwick M, Miao Y. Replacement of the Lys linker with an Arg linker resulting in improved melanoma uptake and reduced renal uptake of Tc-99m-labeled Arg-Gly-Asp-conjugated alpha-melanocyte stimulating hormone hybrid peptide. Bioorg Med Chem. 2010;18: 6695–700. 10.1016/j.bmc.2010.07.061 [PubMed: 20728365]

[117]. Yang J, Lu J, Miao Y. Structural modification on the Lys linker enhanced tumor to kidney uptake ratios of 99mTc-labeled RGD-conjugated α-MSH hybrid peptides. Mol Pharm. 2012;9(5):1418–24. 10.1021/mp2006642 [PubMed: 22452443]

[118]. Yang J, Hu CA, Miao Y. Tc-99m-labeled RGD-conjugated alpha-melanocyte stimulating hormone hybrid peptides with reduced renal uptake. Amino Acids. 2015;47(4):813–23. 10.1007/s00726-014-1911-z [PubMed: 25557051]

[119]. Yang J, Miao Y. Substitution of Gly with Ala enhanced the melanoma uptake of technetium-^{99m}-labeled Arg-Ala-Asp-conjugated alpha-melanocyte stimulating hormone peptide. Bioorg Med Chem Lett. 2012;22(4):1541–5. 10.1016/j.bmcl.2012.01.003 [PubMed: 22297112]

[120]. Flook AM, Yang J, Miao Y. Evaluation of new Tc-99m-labeled Arg-X-Asp-conjugated α-melanocyte stimulating hormone peptides for melanoma imaging. Mol Pharm. 2013;10(9):3417–24. 10.1021/mp400248f [PubMed: 23885640]

[121]. Flook AM, Yang J, Miao Y. Effects of amino acids on melanoma targeting and clearance properties of Tc-99m-labeled Arg-X-Asp-conjugated α-melanocyte stimulating hormone peptides. J Med Chem. 2013;56(21):8793–802. 10.1021/jm4012356 [PubMed: 24131154]

[122]. Flook AM, Yang J, Miao Y. Substitution of the Lys linker with the β-Ala linker dramatically decreased the renal up-take of ^{99m}Tc-labeled Arg-X-Asp-conjugated and X-Ala-Asp-conjugated α-melanocyte stimulating hormone peptides. J Med Chem. 2014;57(21):9010–8. 10.1021/jm501114v [PubMed: 25290883]

[123]. Bernard B, Capello A, Hagen M, Breeman W, Srinivasan A, Schmidt M, et al. Radiolabeled RGD-DTPA-Tyr3-octreotate for receptor-targeted radionuclide therapy. Cancer Biother Rad. 2004;19(2):173–80. 10.1089/108497804323071940

[124]. Capello A, Krenning EP, Bernard BF, Breeman WAP, Mpv H, Jong M. Increased cell death after therapy with an Arg-Gly-Asp-linked somatostatin analog. J Nucl Med. 2004;45: 1716–20. [PubMed: 15471839]

[125]. Capello A, Krenning EP, Bernard BF, Breeman WAP, Erion JL, Jong M. Anticancer activity of targeted proapoptotic peptides. J Nucl Med. 2006;47:122–9. [PubMed: 16391196]

[126]. Shallal HM, Minn I, Banerjee SR, Lisok A, Mease RC, Pomper MG. Heterobivalent agents targeting PSMA and integrin-αvβ3. Bioconjugate Chem. 2014;25(2):393–405. 10.1021/bc4005377

[127]. Zhao J, Guercio BJ, Sahasrabudhe D. Current trends in chemotherapy in the treatment of metastatic prostate cancer. Cancers. 2023;15:3969. 10.3390/cancers15153969 [PubMed: 37568784]

[128]. Verhoeven M, Ruigrok EAM, van Leenders G, van den Brink L, Balcioglu HE, van Weerden WM, et al. GRPR versus PSMA: expression profiles during prostate cancer progression demonstrate the added value of GRPR-targeting theranostic approaches. Front Oncol. 2023;13:1199432. 10.3389/fonc.2023.1199432 [PubMed: 37719014]

[129]. Eder M, Schäfer M, Bauder-Wüst U, Haberkorn U, Eisenhut M, Kopka K. Preclinical evaluation of a bispecific low-molecular heterodimer targeting both PSMA and GRPR for improved PET imaging and therapy of prostate cancer. Prostate. 2014;74(6):659–68. 10.1002/pros.22784 [PubMed: 24464532]

[130]. Bandari RP, Lewis MR, and Smith CJ. Synthesis and evaluation of [DUPA-6-Ahx-Lys (DOTA)-6-Ahx-RM2], a novel, bivalent targeting ligand for GRPr/PSMA biomarkers of prostate cancer. 2018;5:14.

[131]. Mendoza-Figueroa MJ, Escudero-Castellanos A, Ramirez-Nava GJ, Ocampo-García BE, Santos-Cuevas CL, Ferro-Flores G, et al. Preparation and preclinical evaluation of 68Ga-iPSMA-BN as a potential heterodimeric radiotracer for PET-imaging of prostate cancer. J Radioanal Nucl Chem. 2018;318:2097–105.

[132]. Rivera-Bravo B, Ramírez-Nava G, Mendoza-Figueroa MJ, Ocampo-García B, Ferro-Flores G, Ávila-Rodríguez MA, et al. [^{68}Ga]Ga-iPSMA-Lys(3)-Bombesin: biokinetics, dosimetry and first patient PET/CT imaging. Nucl Med Biol. 2021;96–97:54–60.

[133]. Mitran B, Varasteh Z, Abouzayed A, Rinne SS, Puuvuori E, De Rosa M, et al. Bispecific GRPR-antagonistic anti-PSMA/GRPR heterodimer for PET and SPECT diagnostic imaging of prostate cancer. Cancers. 2019;11:1371. [PubMed: 31540122]

[134]. Liolios C, Schäfer M, Haberkorn U, Eder M, Kopka K. Novel bispecific PSMA/GRPr targeting radioligands with optimized pharmacokinetics for improved PET imaging of prostate cancer. Bioconjugate Chem. 2016;27:737–51.

[135]. Bandari RP, Lewis MR, Smith CJ. Synthesis and evaluation of [DUPA-6-Ahx-Lys (DOTA)-6-Ahx-RM2], a novel, biva-lent targeting ligand for GRPr/PSMA biomarkers of prostate cancer. Chem Biol Lett. 2018;5:14.

[136]. Bailly T, Bodin S, Goncalves V, Denat F, Morgat C, Prignon A, et al. Modular one-pot strategy for the synthesis of heterobivalent tracers. ACS Med Chem Lett. 2023;14:636–44. [PubMed: 37197474]

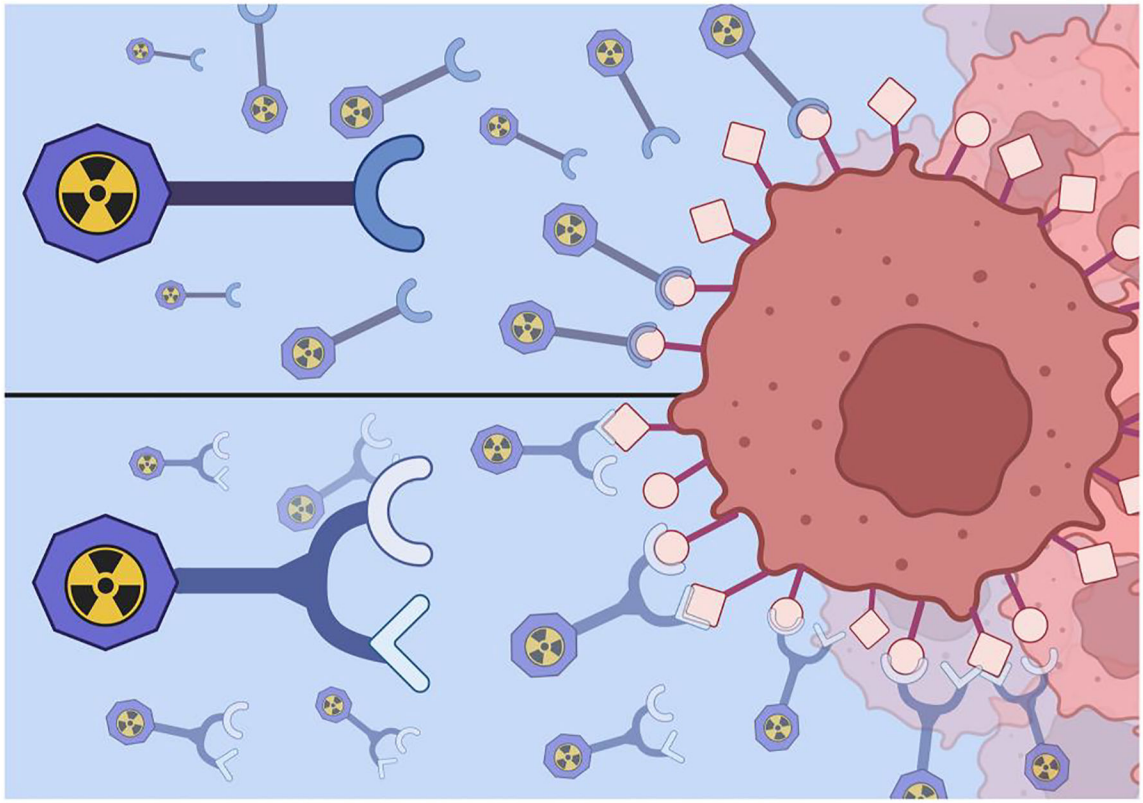

FIGURE 1.
Basic design comparison of a monovalent radiopharmaceutical (top) compared to a bivalent radiopharmaceutical (bottom) targeting receptors on a cancer cell. Created with BioRender.com.

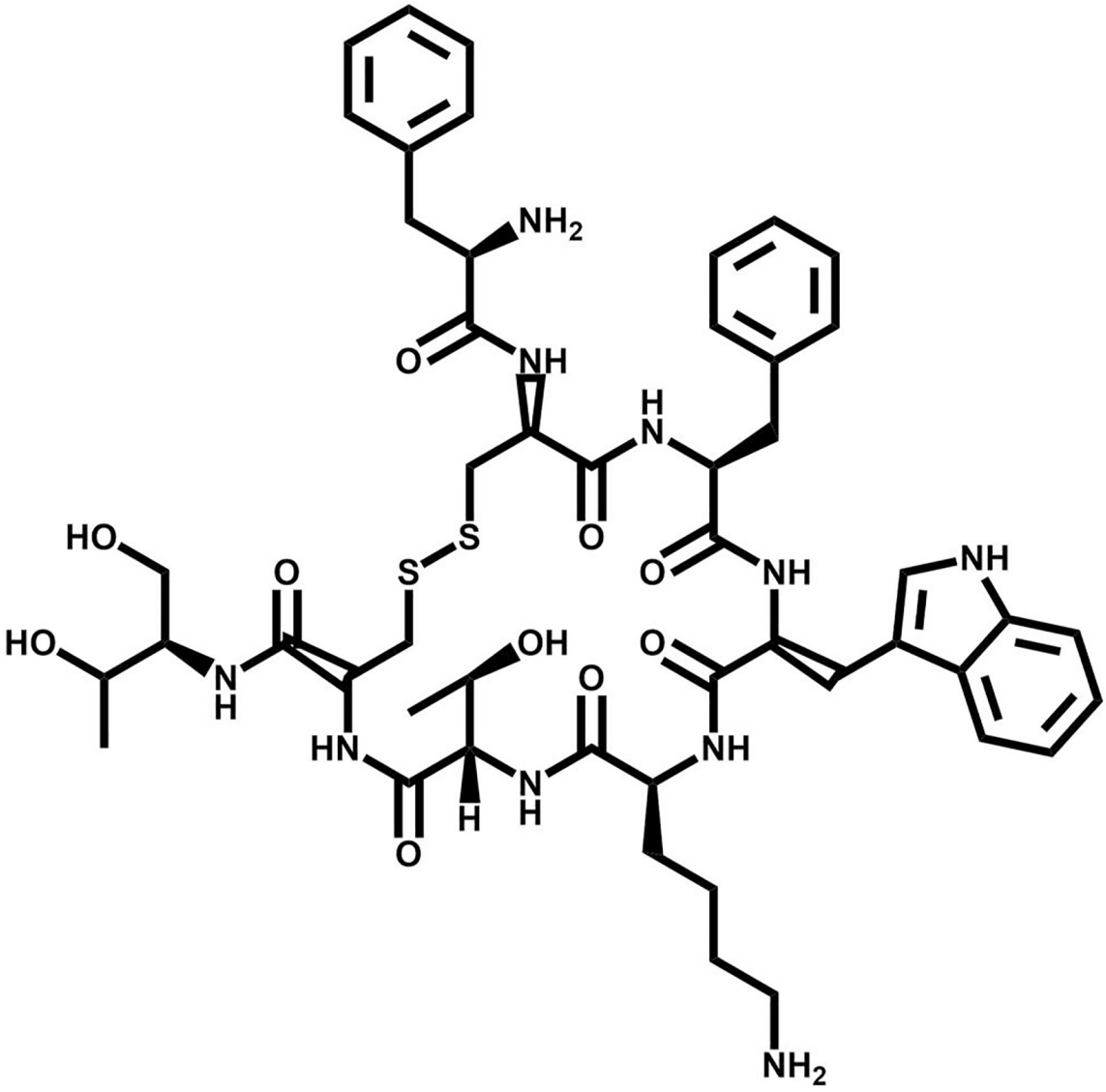

FIGURE 2.
The chemical structure of octreotide, a somatostatin (SST) targeting vector.

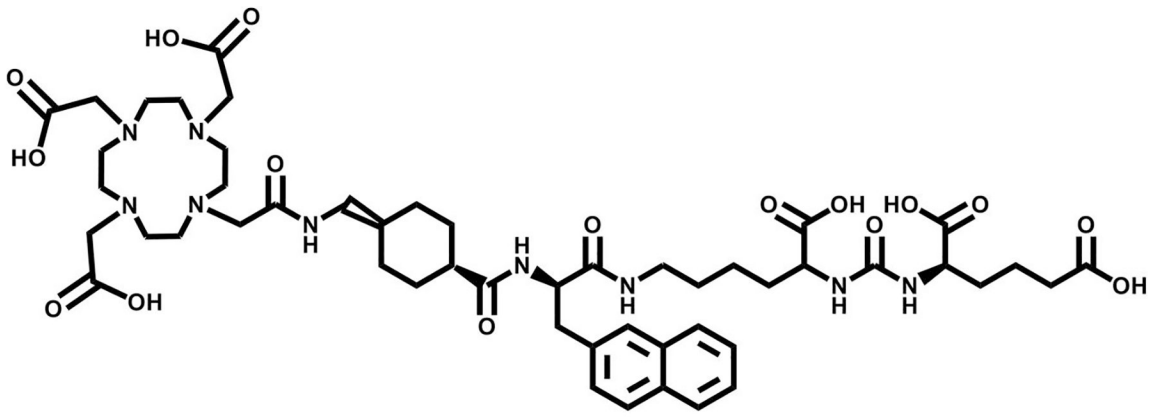

FIGURE 3.

The chemical structure of PSMA-617, a prostate specific membrane antigen (PSMA) targeting vector.

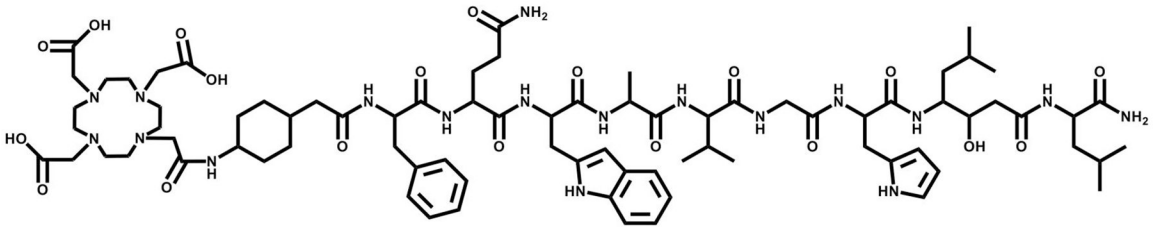

FIGURE 4.

The chemical structure of DOTA-RM2, a gastrin releasing peptide receptor (GRPR) targeting vector.

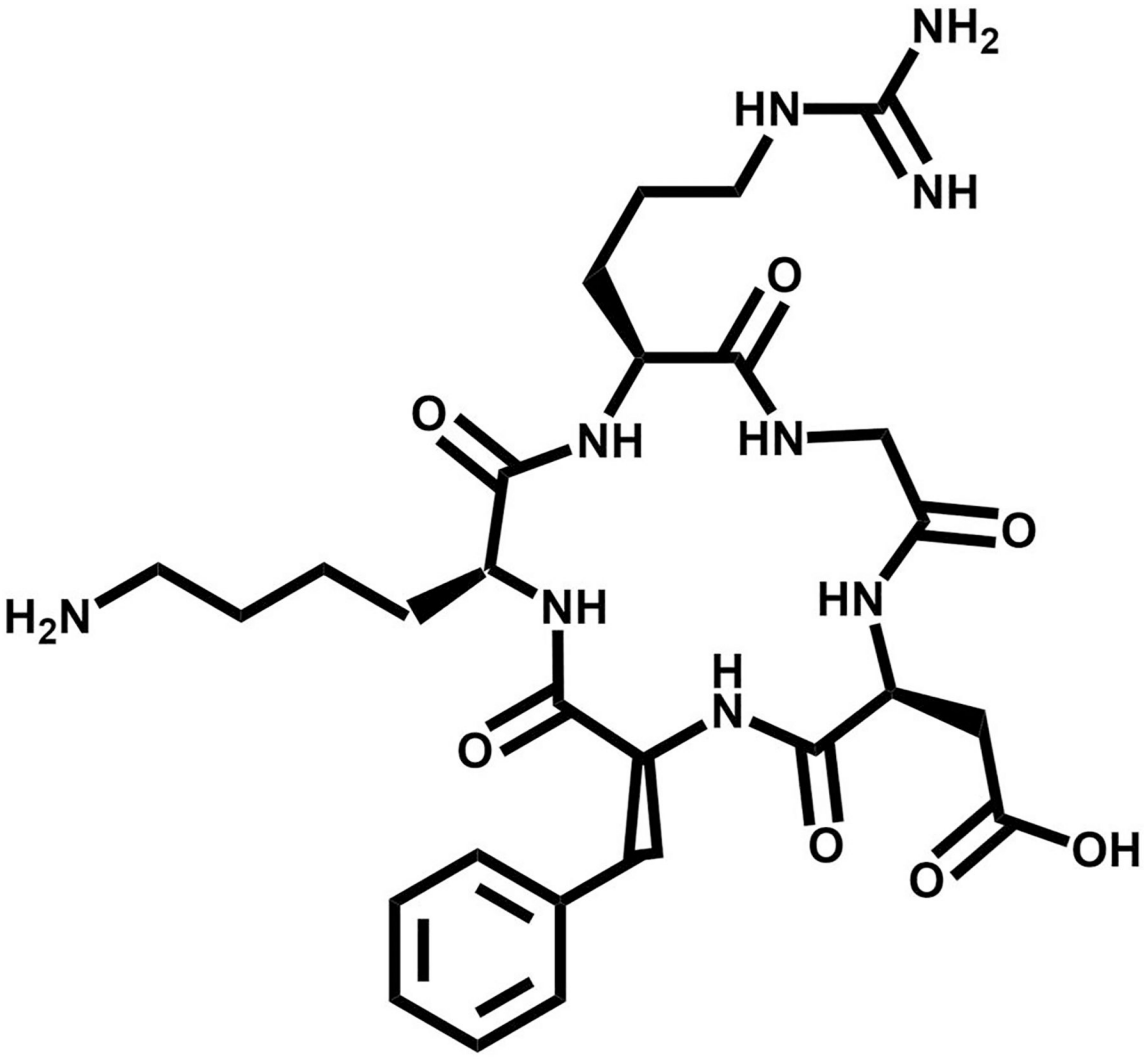

FIGURE 5.
The chemical structure of c[RGDfK], an $\alpha_v\beta_3$ targeting vector.

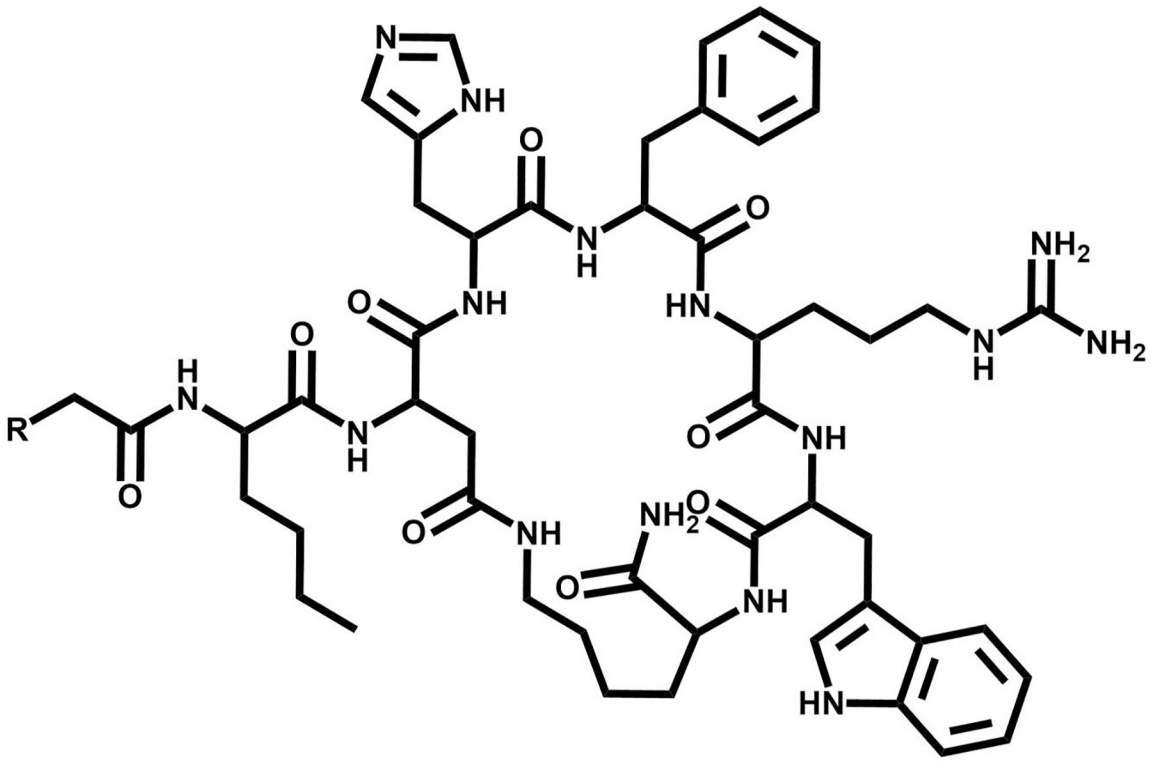

FIGURE 6.

The chemical structure of Nle-CycMSH$_{hex}$, an MC1R targeting vector where *R* denotes complexing agent.

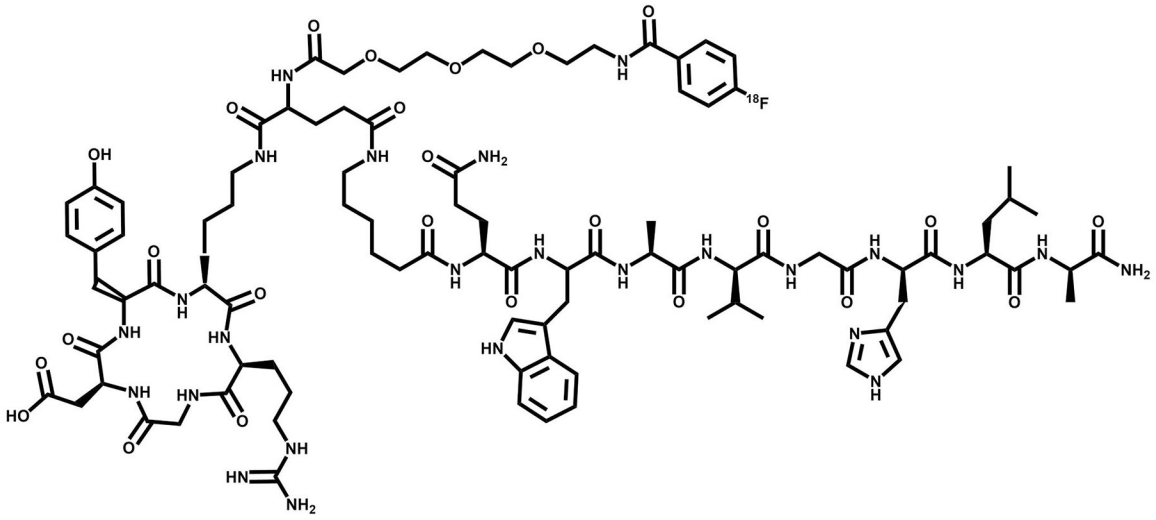

FIGURE 7.
Structure of 18F labeled FB-PEG2-Glu-RGD-BBN, a heterobivalent $\alpha_v\beta_3$-GRPR targeting peptide

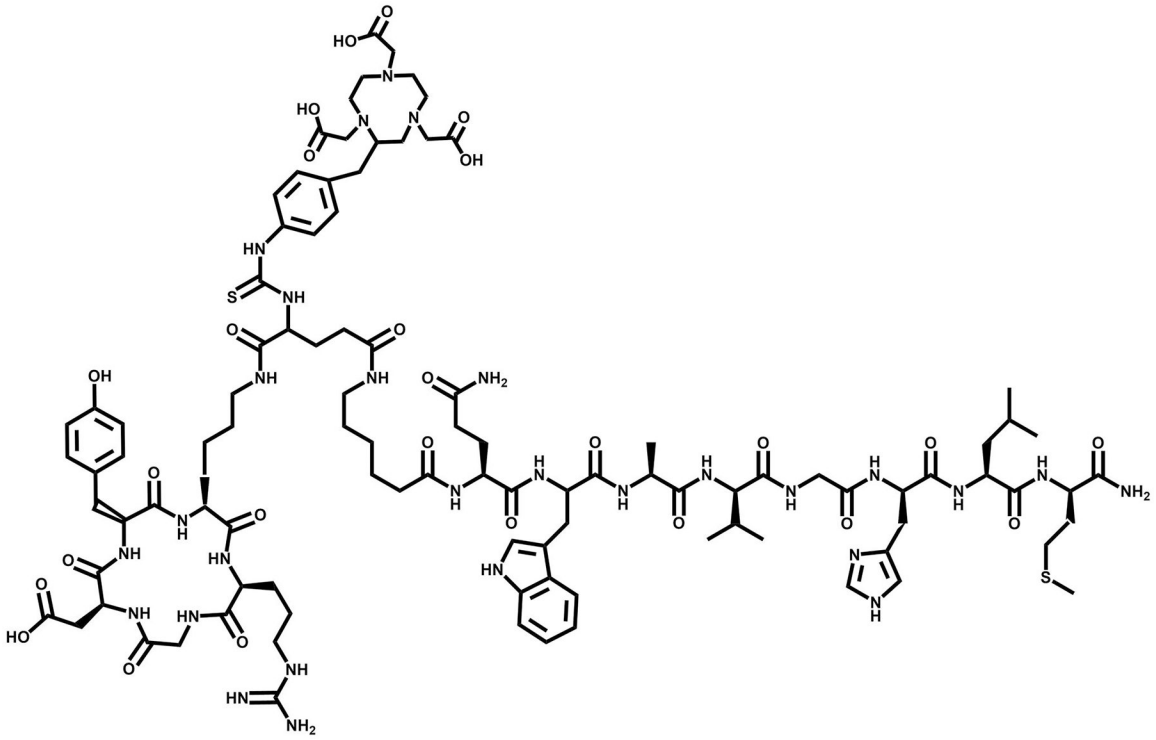

FIGURE 8.
Structure of NOTA-RGD-BBN, a heterobivalent $\alpha_v\beta_3$-GRPR targeting peptide.

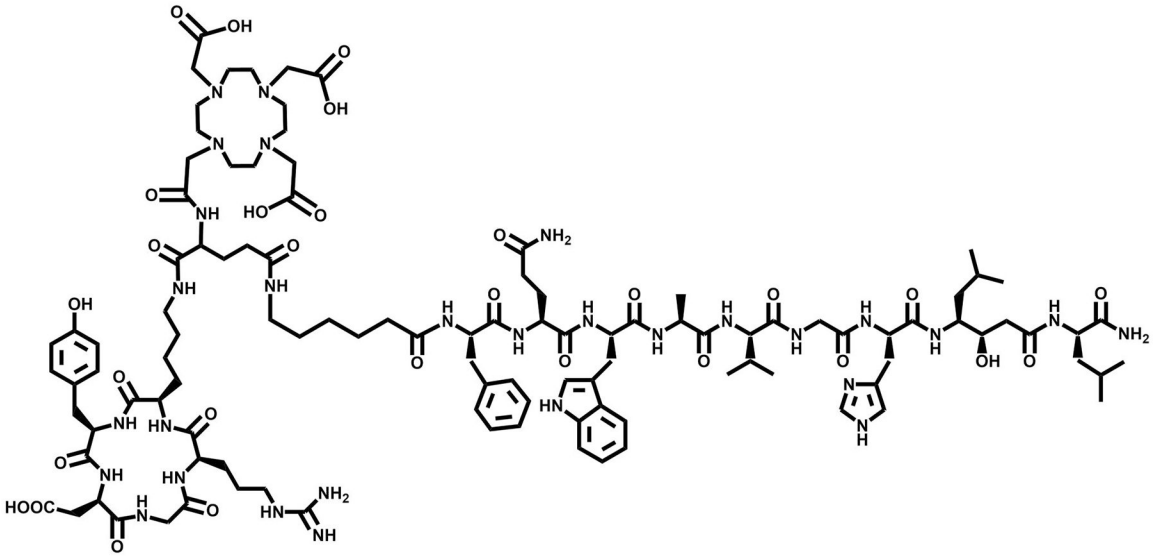

FIGURE 9.
Structure of RGD-Glu-(DO3A)-6-Ahx-RM2, a heterobivalent $\alpha_v\beta_3$-GRPR targeting peptide.

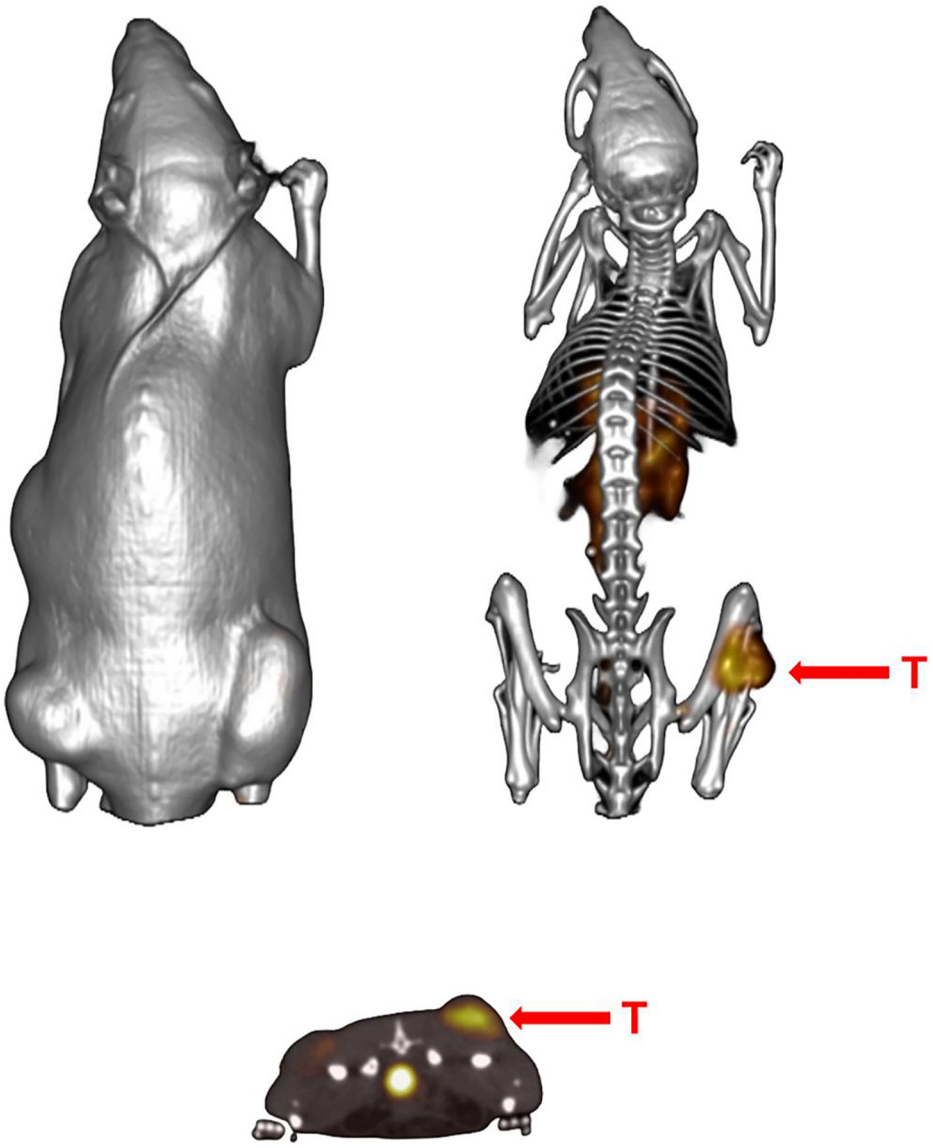

FIGURE 10.

Maximum intensity small animal single-photon emission tomography (SPECT) (tumor) and CT (skeletal) fusion coronal whole-body images of PC-3 tumor bearing SCID mouse after 18 h tail vein injection of [67Ga-DO3A]-BBN ANT-RGD] heterodimer. [105] Tumor uptake at the 1 h time-point was 10.86%ID/g with retention of 4.09%ID/g at 24 h p.i. Tumors are denoted by red arrows.

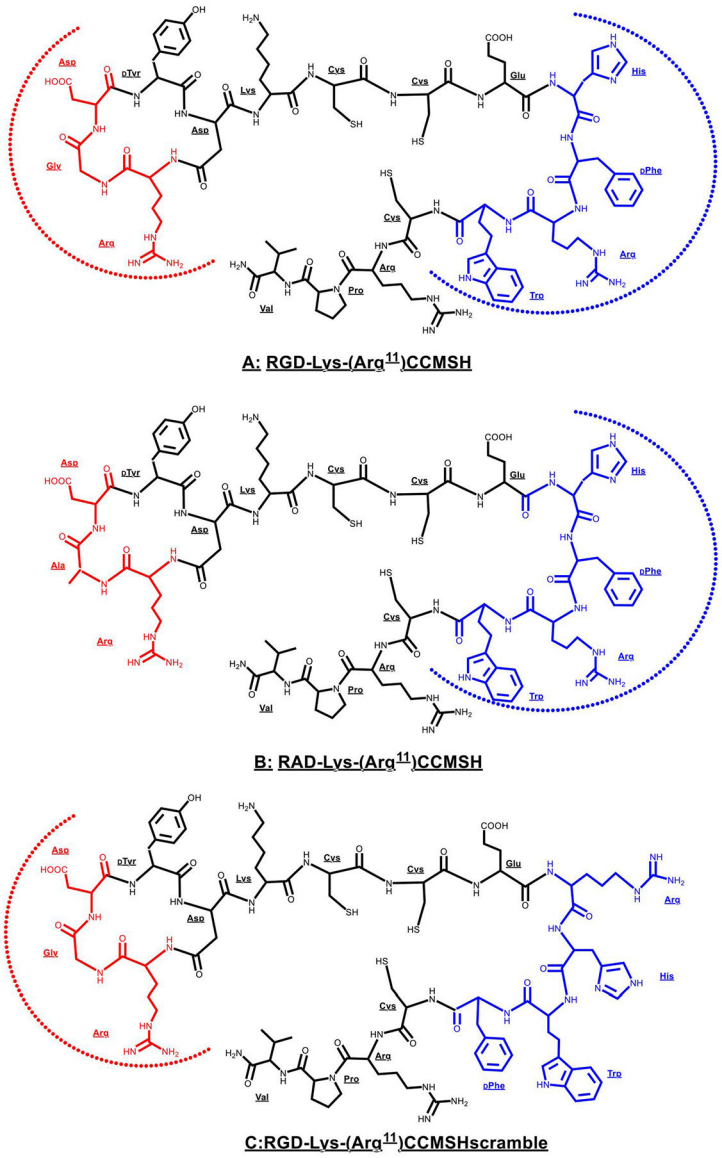

FIGURE 11.

Schematic structures of RGD-Lys-(Arg^{11})CCMSH (a), RAD-Lys-(Arg^{11})CCMSH (b) and RGD-Lys-(Arg^{11})CCMSH$_{scramble}$ (c) hybrid peptides. The receptor binding sequences were highlighted with dashed half circles. Reproduced with permission from ref. [114].

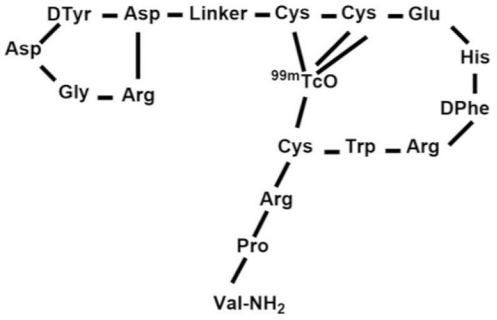

Peptide	Linker Structure	M21 Melanoma Uptake (%ID/g at 2 h PI)	Renal Uptake in M21 Tumor-Bearing Nude Mice (%ID/g at 2 h PI)
^{99m}Tc-RGD-Lys-(Arg^{11})CCMSH	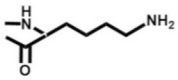	2.69 ± 0.78	67.06 ± 16.53
^{99m}Tc-RGD-Aoc-(Arg^{11})CCMSH	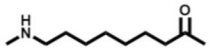	2.35 ± 0.12	27.93 ± 3.98
^{99m}Tc-RGD-PEG$_2$-(Arg^{11})CCMSH	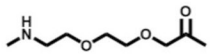	1.71 ± 0.25	22.01 ± 9.89

Peptide	Linker Structure	B16/F1 Melanoma Uptake (%ID/g at 2 h PI)	Renal Uptake in B16/F1 Tumor-Bearing C57 Mice (%ID/g at 2 h PI)
^{99m}Tc-RGD-Lys-(Arg^{11})CCMSH	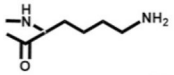	14.83 ± 2.94	67.12 ± 8.79
^{99m}Tc-RGD-Arg-(Arg^{11})CCMSH	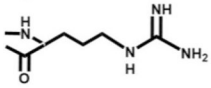	21.41 ± 3.74	43.01 ± 8.14
^{99m}Tc-RGD-Ahx-(Arg^{11})CCMSH	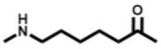	11.85 ± 1.95	16.88 ± 1.82
^{99m}Tc-RGD-bAla-(Arg^{11})CCMSH	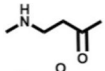	14.67 ± 0.78	16.31 ± 4.60
^{99m}Tc-RGD-Gly-(Arg^{11})CCMSH		11.50 ± 1.01	20.85 ± 4.51
^{99m}Tc-RGD-(Arg^{11})CCMSH	No linker	16.12 ± 3.09	23.88 ± 1.45

FIGURE 12.

The melanoma and renal uptake of ^{99m}Tc-RGD-Linker-(Arg^{11})CCMSH peptides at 2 h post-injection in M21 human melanoma-xenografted nude mice and B16/F1 murine melanoma-bearing C57 mice.

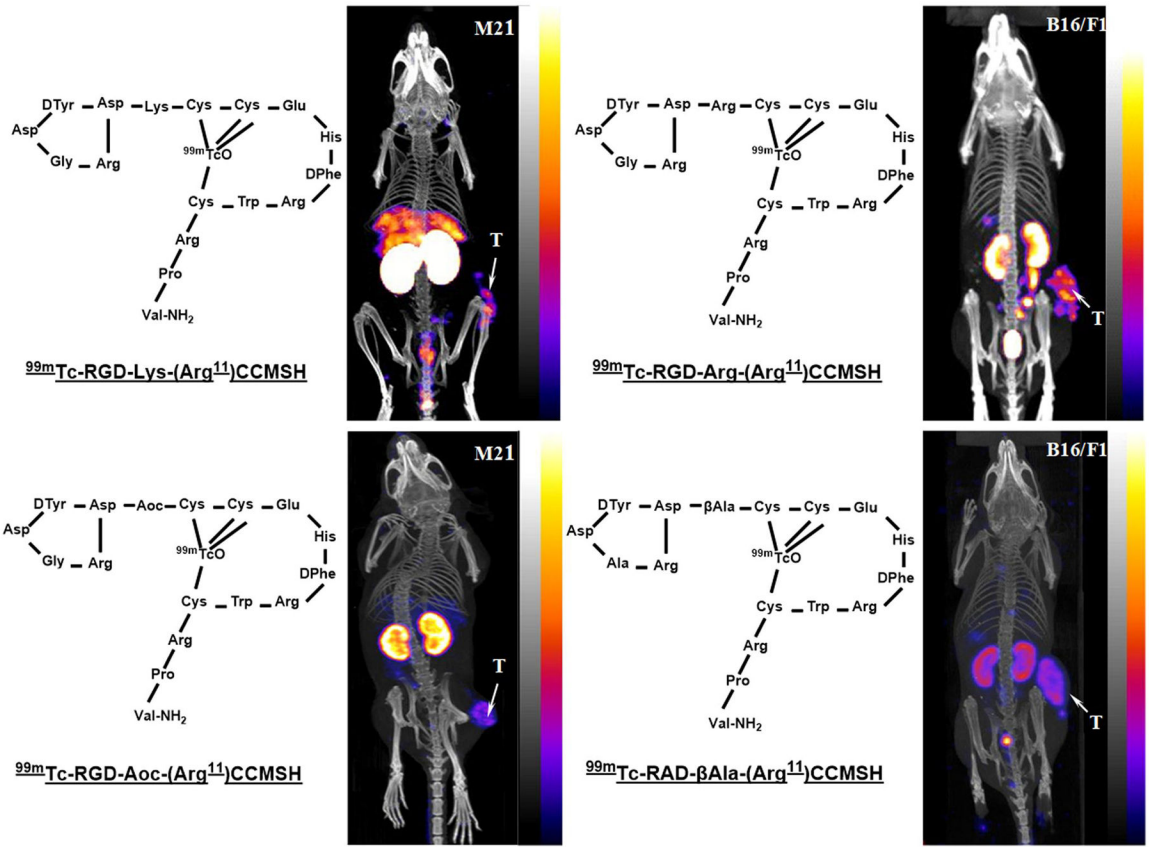

FIGURE 13.

Maximum intensity projection single-photon emission tomography (SPECT)/CT images of ^{99m}Tc-RGD-Lys-(Arg^{11}) CCMSH and ^{99m}Tc-RGD-Aoc-(Arg^{11})CCMSH on M21 human melanoma-xenografted nude mice (left), ^{99m}Tc-RGD-Arg-(Arg^{11})CCMSH and ^{99m}Tc-RAD-βAla-(Arg^{11})CCMSH on B16/F1 melanoma-bearing C57 mice (right) at 2 h post-injection, respectively. Reproduced with permission from ref. [114, 115, 116, 122].

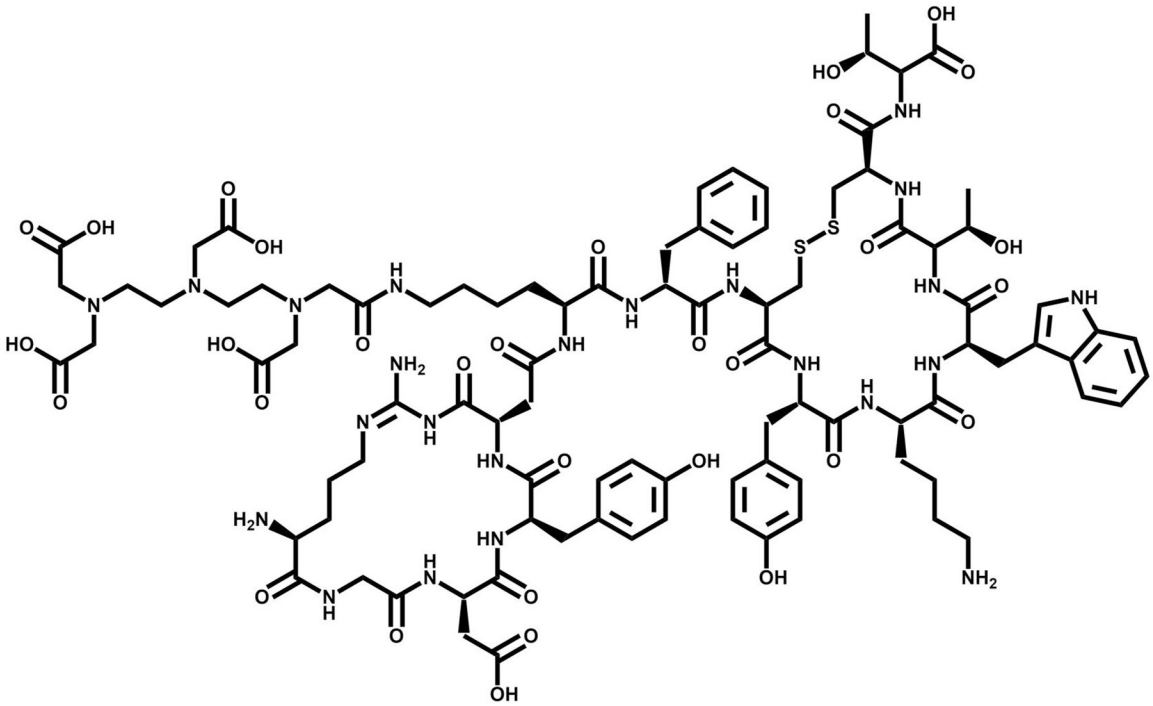

FIGURE 14.
Structure of RGD-DTPA-Tyr3-octreotate, a heterobivalent αvβ3-SST2 targeting vector.

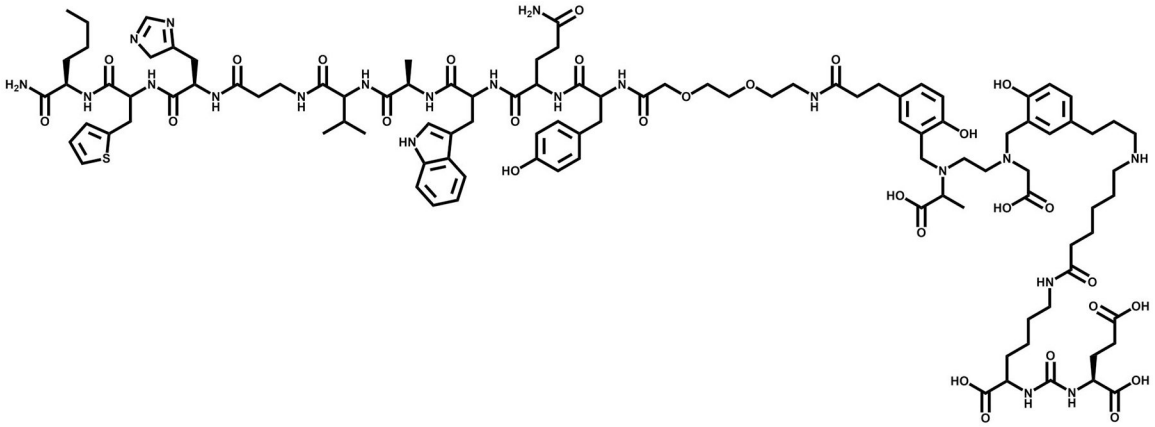

FIGURE 15.
Structure of Glu-urea-Lys(Ahx)-HBED-CC-BZH3, a heterobivalent PSMA-GRPR targeting vector.

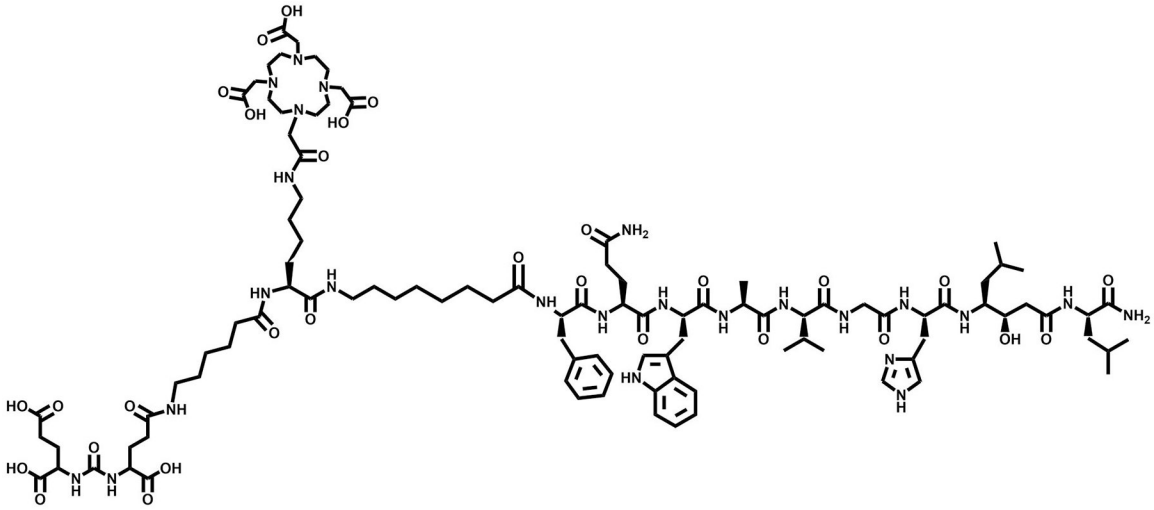

FIGURE 16.
Structure of [DUPA-6-Ahx-Lys(DOTA)-6-Ahx-RM2], a heterobivalent PSMA-GRPR targeting vector.

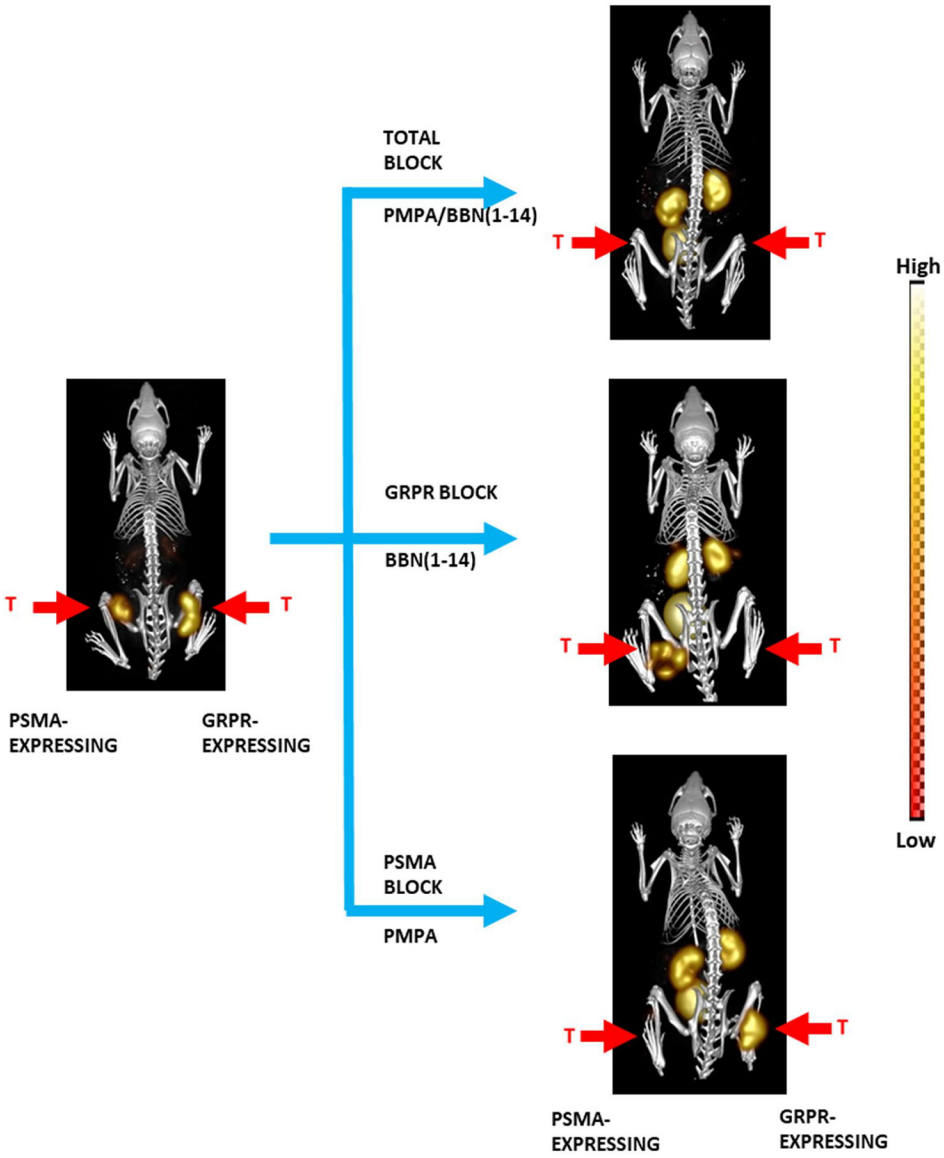

FIGURE 17.

[DUPA-6-Ahx-(DOTA)-8-Aoc-BBN ANT] radiolabeled with ^{111}In in PC-3 and PC-PIP tumor-bearing SCID mice at 4 h post-tail vein injection of bilateral xenografted tumors. Whole-body images are maximum-intensity microSPECT registered to microCT. The ^{111}In labeled conjugate had uptake values of 4.74 ± 0.90%ID/g in PC3 tumors and 5.38 ± 1.07%ID/g in PC3-PIP tumors. Tumors are denoted by red arrows.

TABLE 1

Common metal-based radionuclides for either molecular imaging (**γ** or **β**$^{+}$) or targeted radiotherapy (TRT) (**β**$^{-}$ or **α**).

Radionuclide	Production	Decay	Half life ($T_{1/2}$)	$E^{+/-}$ (MeV)	Application
^{64}Cu	^{64}Ni(p,n)^{64}Cu	EC, β^-, β^+	12.7 h	**γ**: 1.3458 **β**$^{-}$: 0.578 **β**$^{+}$: 0.651	Diagnostic
^{67}Cu	^{68}Zn(γ,p)^{67}Cu	β^-, γ	61.8 h		Therapeutic
^{68}Ga	^{68}Ge/^{68}Ga Generator	EC, β^+	67.7 min	**γ**: 1.0773 **β**$^{+}$: 1.899	Diagnostic
^{86}Y	^{86}Sr(p,n)^{86}Y	EC, β^+	14.74 h	**γ**: 1.0767, 0.6278, 1.153.1 **β**$^{+}$: 1.248	Diagnostic
^{89}Zr	^{89}Y(p,n)^{89}Zr	EC, β^+, γ	78.4 h	**γ**: 0.909, 1.713, 1.657 **β**$^{+}$: 0.897	Diagnostic
^{90}Y	^{90}Sr/^{90}Y Generator	β^-	64.2 h	**β**$^{-}$: 2.27	Therapeutic
^{99m}Tc	^{99}Mo/^{99m}Tc Generator	IT	6.1 h	**γ**: 0.1427	Diagnostic
^{111}In	^{112}Cd(p,2n)^{111}In	EC	67.2 h	**γ**: 0.1713, 0.2454	Diagnostic
^{153}Sm	^{152}Sm(n,γ)^{153}Sm	β^-, γ	46.3 h	**β**$^{-}$: 0.69, 0.64 **γ**: 0.1032, 0.0697	Therapeutic
^{166}Ho	^{165}Ho(n,γ)^{166}Ho	β^-, γ	26.8 h	**β**$^{-}$: 1.855, 1.773 **γ**: 0.0806, 1.3794	Therapeutic
^{177}Lu	^{176}Lu(n,γ)^{177}Lu	β^-, γ	6.65 d	**β**$^{-}$: 0.497 **γ**: 0.2084, 0.1129	Therapeutic, diagnostic
^{186}Re	^{185}Re(n,γ)^{186}Re	β^-, γ	3.8 d	**β**$^{-}$: 1.071, 0.933 **γ**: 0.1372	Therapeutic
^{211}At	^{209}Bi(α,2n)^{211}At	EC, α, γ	7.21	**γ**: 0.1372 **α**: 5.868	Therapeutic
^{203}Pb	^{203}Tl(p,n)^{203}Pb	Γ	51.9 h	**γ**: 279.2	Diagnostic
^{212}Pb	^{224}Ra/^{212}Pb Generator	β^-, γ	10.6 h	**β**$^{-}$: 0.569, 0.335 **γ**: 0.3000, 0.2386	Therapeutic

TABLE 2

A brief outline of $\alpha_v\beta_3$-GRPR receptor-targeting radiotracers.

Compound name	Isotope	Reference number
RGD-BBN	^{18}F	[93]
NOTA-RGD-BBN	^{68}Ga, ^{64}Cu	[97, 98]
FB-PEG_3-Glu-RGD-BBN	^{18}F	[98]
DO3A-RGD-BBN	^{177}Lu	[94]
NO2A-RGD-Glu-6-Ahx-BBN (7–14)NH2	^{64}Cu	[95]
RGD-Glu-[NO2A]-6-Ahx-RM2	^{64}Cu	[5]
RGD-Glu-[DO3A]-6-Ahx-RM2	^{111}In, ^{177}Lu	[96]

TABLE 3

A brief outline of $\alpha_v\beta_3$-MC1R receptor-targeting radiotracers.

Compound name	Isotope	Reference number
RGD-X-(Arg^{11})CCMSH X = Lys, PEG_2, Arg, Ahx, βAla, Gly	^{99m}Tc	[114–118]
RXD-Lys-(Arg^{11})CCMSH X = Thr, Val, Ser, Nle, Phe, DPhe	^{99m}Tc	[119, 121]

TABLE 4

A brief outline of $\alpha_v\beta_3$-SST2 receptor-targeting radiotracers.

Compound name	Isotope	Reference number
RGD-DTPA-Tyr^3-octreotate	^{111}In	[123]
RGD-DOTA-Tyr^3-octreotide	^{111}In	[123]

TABLE 5

A brief outline of PSMA-GRPR receptor-targeting radiotracers.

Compound name	Isotope	Reference number
Glu-urea-Lys(Ahx)-HBED-CC-BZH3	^{68}Ga	[129]
[DUPA-6-Ahx-(NODAGA)-5-Ava-BBN (7–14)NH_2	^{64}Cu	[4]
[DUPA-6-Ahx-Lys(DOTA)-6-Ahx-RM2]	^{67}Ga, ^{111}In, ^{177}Lu	[130]
[DUPA-6-Ahx-Lys(DOTA)-8-Aoc-RM2]	^{111}In, ^{177}Lu	[3]
Glu-CO-Lys[2Nal-Cys[Lys^3(GMBS)-BBN-NH_2]-DOTA] (iPSMA-BN)	^{68}Ga	[131, 132]
NOTA-DUPA-RM26	^{111}In, ^{68}Ga	[133]